Applied Energy 267 (2020) 114903

Contents lists available at ScienceDirect

Applied Energy

journal homepage: www.elsevier.com/locate/apenergy

A framework for the optimal integration of solar assisted district heating in different urban sized communities: A robust machine learning approach incorporating global sensitivity analysis

Mohamed Hany Abokersh[a], Manel Vallès[a], Luisa F. Cabeza[b], Dieter Boer[a,*]

[a] Departament d'Enginyeria Mecànica, Universitat Rovira i Virgili, Av. Països Catalans 26, 43007 Tarragona, Spain
[b] GREiA Research Group, INSPIRES Research Centre, Universitat de Lleida, Pere de Cabrera s/n, 25001 Lleida, Spain

HIGHLIGHTS

- A framework to assess the sustainability of solar district heating system is framed.
- A robust ANN model to solve the computational cost with TRNSYS models is developed.
- Multi-objective optimization is carried out for four sizes of solar communities.
- The effect of storage construction variety is tested in the optimization problem.
- Global Sensitivity Analysis to identify the uncertain parameters is proposed.

GRAPHICAL ABSTRACT

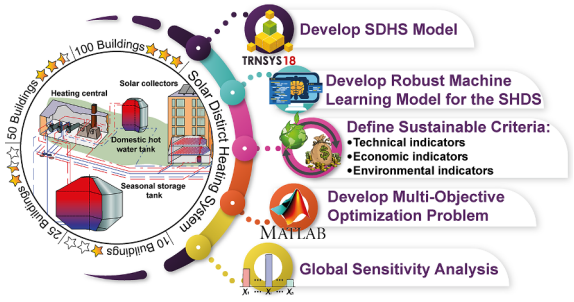

ARTICLE INFO

Keywords:
Solar assist district heating system
Artificial Neural Network
Bayesian optimization approach
Life cycle assessment
Multi-objective optimization
Global sensitivity analysis

ABSTRACT

A promising pathway towards sustainable transaction to clean energy production lies in the adoption of solar assisted district heating systems (SDHS). However, SDHS technical barriers during their design and operation phases, combined with their economic limitation, promote a high variation in quantifying SDHS benefits over their lifetime. This study proposes a complete multi-objective optimization framework using a robust machine learning approach to inherent sustainability principles in the design of SDHS. Moreover, the framework investigates the uncertainty in the context of SDHS design, in which the Global Sensitivity Analysis (GSA) is combined with the heuristics optimization approach. The framework application is illustrated through a case study for the optimal integration of SHDS at different urban community sizes (10, 25, 50, and 100 buildings) located in Madrid. The results reveal a substantial improvement in economic and environmental benefits for deploying SDHS, especially with including the seasonal storage tank (SST) construction properties in the optimization problem, and it can achieve a payback period up to 13.7 years. In addition, the solar fraction of the optimized SDHS never falls below 82.1% for the investigated community sizes with an efficiency above 69.5% for the SST. Finally, the GSA indicates the SST investment cost and its relevant construction materials, are primarily responsible for the variability in the optimal system feasibility. The proposed framework can provide a good starting point to solve the enormous computational expenses drawbacks associated with the heuristics optimization approach. Furthermore, it can function as a decision support tool to fulfill the European Union energy targets regarding clean energy production.

* Corresponding author.
E-mail addresses: mohamed.abokersh@urv.cat (M.H. Abokersh), manel.valles@urv.cat (M. Vallès), lcabeza@diei.udl.cat (L.F. Cabeza), dieter.boer@urv.cat (D. Boer).

https://doi.org/10.1016/j.apenergy.2020.114903
Received 11 November 2019; Received in revised form 12 March 2020; Accepted 26 March 2020
Available online 13 April 2020

Nomenclature

A_{COL}	total aperture area of solar collectors (m^2/MWh/a)
β_{COL}	inclination angle of the solar collectors (°)
C_C	total initial capital cost (€)
C_O	total discounted operational cost (€)
C_R	total discounted replacement cost (€)
CAP_k	design variable of equipment unit k
$CEPCI^{year\ A}$	chemical engineering plant cost index in the base year
$CEPCI^{year\ B}$	Chemical Engineering Plant Cost Index in the installation year
Con_{SST}	purchase cost of the construction material of the seasonal storage tank (€)
C_M	annual cost of equipment unit k (€)
C_P	annual operational cost of a pump (€)
c_p	specific heat capacity (kJ/kg. k)
c_e	electricity price (€)
c_f	natural gas price (€)
$C.V$	coefficient of variation (%)
d	annual discount rate (%)
d_{Roof}	insulation material thickness for the seasonal storage tank roof (m)
d_{Wall}	insulation material thickness for the seasonal storage tank wall (m)
d_{Gnd}	insulation material thickness for the seasonal storage tank ground (m)
DAM_d	indicator result for damage category$d$
FBM_k	bare module factor of equipment unit$k$
FC_{AUX}	contribution of the auxiliary heater as a percentage of the maximum heating load (%)
$f_c(x)$	original objective function [NPC(x) or RCP(x)]
HDR	seasonal storage tank aspect ratio (m/m)
HDR_{DHWT}	domestic hot water storage aspect ratio (m/m)
i	annual inflation rate (%)
i_f	annual inflation rate of natural gas (%)
i_e	annual inflation rate of electricity (%)
Ins_{SST}	purchase cost of the insulation materials of the seasonal storage tank (€)
k	number of regressors
$\dot{m}$	mass flowrate of the recirculating water pumps (kg/s)
n	sample size
N_{COL}	number of solar collectors in series
NPC	net present cost (€/MWh)
PEC_k	purchase cost of equipment unit k (€)
PWF_n	present worth factor of periodic future cash flows (–)
PVF_n	present value factor of single future cash flow at the beginning of n^{th} time period (–)
$\dot{Q}_{SOL}$	useful energy rate received by the solar collector field (MW)
$\dot{Q}_{SST\ loss}$	heat loss rate through the seasonal storage tank (MW)
$\dot{Q}_{DHW\ loss}$	heat loss rate through the domestic hot water storage tank (MW)
$\dot{Q}_{HE}$	heat transfer rate through the heat exchanger (MW)
$\dot{Q}_{AUX}$	duty of auxiliary heater (MW)
$Q_{SH\ load}$	total space heating demand (MWh)
$Q_{DHW\ load}$	total domestic hot water demand (MWh)
$Q_{SST\ loss}$	total energy losses through the seasonal storage tank (MWh)
$SMAPE$	symmetric mean absolute percentage error
R^2	coefficient of determination
$R^2 - Adj.$	adjusted coefficient of determination
RCP	ReCiPe 2016 aggregated impact factor (Pt/MWh)
$S.F_{DHW}$	annual solar fraction for the DHW distribution circuit (%)
$S.F_{SH}$	annual solar fraction for the SH distribution circuit (%)
U_{Roof}	the heat loss coefficient of the seasonal storage tank roof (W/m^2·K)
U_{Wall}	the heat loss coefficient of the seasonal storage tank wall (W/m^2·K)
U_{Gnd}	the heat loss coefficient of the seasonal storage tank ground (W/m^2·K)
$U_{Overall}$	the overall heat loss coefficient of the seasonal storage tank (W/m^2·K)
V_{DHWT}	volume of the domestic hot water tank (m^3/MWh/a)
V_{SST}	volume of the seasonal storage tank (m^3/MWh/a)
$y_{predict,i}$	predicted value
$y_{data,i}$	actual value

Greek symbols

α_{CF}	factor of contingency charges and fees
α_k	purchase cost coefficient of equipment unitk
β_k	purchase cost exponent of equipment unit k
η_{COL}	solar collector field efficiency (%)
η_{DHWT}	domestic hot water storage tank efficiency (%)
η_{SST}	seasonal storage tank efficiency (%)
λ_{con}	construction material thermal conductivity of the seasonal storage tank (W/m·K)
λ_{ins}	insulation material thermal conductivity for the seasonal storage tank roof and wall (W/m·K)
$\lambda_{ins\ gnd}$	insulation material thermal conductivity for the seasonal storage tank ground (W/m·K)
δ_d	normalization factor for damage category d
ε_d	weighting factor for damage category d
ΔT_{SST}	temperature difference between the extracted and replaced water inside the space heating circuit

Abbreviations

ANN	Artificial Neural Network
AUX	auxiliary heater fueled by natural gas
COL	solar collector field
DHW	domestic hot water
DHWT	domestic hot water storage
DHWcalc	Domestic Hot Water profiles generator software
EPBP	economic payback period
GHG	greenhouse gas
GPBP	greenhouse gas payback period
GSA	global sensitivity analysis
FG	foam glass gravel
HE	heat exchanger
HPC	high-performance concrete
LCA	life cycle assessment
LCC	life cycle cost
LSA	local sensitivity analysis
MILP	mixed-integer linear programming
MINLP	mixed Integer Nonlinear Programming
MOO	multi-objective optimization
MOGA	multi-objective genetic algorithm
MW	mineral wool
NC	normal concrete
P	centrifugal pump
SDHS	solar assisted district heating system

SH	space heating
SST	seasonal storage tank
TES	thermal energy storage
TRNSYS	transient system simulation program
UHPC	ultra-high performance concrete
XPS	extruded polystyrene

Indices

d	damage category
i	elementary factor
k	equipment unit

1. Introduction

Despite the global tendency in shifting the current energy production towards more and sustainable energy options, the carbon dioxide (CO_2) emissions keep growing by 6.5% over the last five years [1].

In Europe, the Governance of the Energy Union approved new clean energy for all Europeans package [2]. This plan comprehensively updates the European Union (EU) energy policy framework to facilitate the sustainable transaction from fossil fuel towards the deployment of renewable energy to follow up the EU 2030 targets for climate and energy consistently with delivering the EU Paris agreement commitments towards the reduction in greenhouse gas emissions (GHG) [3]. An important step to spread on the clean energy transition in the European Union and its Member States is the energy efficiency in the building sector. Buildings represent one of the biggest energy consumers in the EU, accounting for more than 40% of the final energy consumption [4], where the residential buildings consume 63% of this energy [5]. Moreover, more than 75% of residential energy consumption is utilized for space and domestic hot water heating [6]. Along with all these figures, the residential sector counts for about 10% of the total GHG in 2017 [7]. In response to this issue, the EU promoted the Energy Efficiency Directive plan 2012/27/EU [8]. This plan tends to boost the energy performance of the buildings and introduce energy certificates, taking into account the external climatic conditions and defining Net Zero Energy Buildings. Even though these actions plan led to decrease the final energy consumption of the residential section by 9.3% over the last 15 years, still the average energy consumption still increases by 0.4% per year due to the growth in the urbanization area and dispersion of the central heating [9]. Aligning with this growth, various types of renewable energy systems are installed in the building sector for electricity and thermal loads coverage.

Among all renewable sources, solar energy seems to be the most promising alternative for fossil fuel due its unique benefits [10]. However, the main drawback of solar thermal energy, as well as the other renewable energy sources, is the intermittency and fluctuation based on short and long term basis [11,12], which causes a gap between the energy demand and supply. Between several storage techniques, the thermal energy storage (TES) systems seem to be the most promising technologies that fulfill this gap issue. TES systems store the excess generated power and provides it on-demand [13]. Considering their storage capacity, TES systems comprise two main categories; these categories are short- and long-term systems. Short-term systems have a charge-discharge capacity for a few days and they are widely known as diurnal storage [14]. In general, these systems suffer from demand coverage problems during the winter season, especially in the high latitude countries. This is due to the difference in solar availability between summer and winter seasons [15]. On the other hand, long-term storage can last up for several months, and it is known as seasonal TES. Accordingly, seasonal TES can efficiently contribute to solve the demand issue during the winter season, and consequently improve the usage of renewable energy source in district heating systems aligning with the building decarbonization concept [16,17]. Even though seasonal TES has been developed for chemical and latent heat storage, the existing seasonal TES mainly uses sensible storage due to its stability [18].

In Europe, the begin of developing solar assisted district heating systems (SDHS) coupled with sensible seasonal TES began in the 1970s with the energy crisis [19]. Such district heating communities have been established in the 1990s and 2000s, mostly in Denmark and Germany [20]. Since then, the SHDS market has been growing practically in Northern and Central Europe [21]. With few exceptions (detailed below), the real performance of the SDHS has met with the estimated or predicted results. In Friedrichshafen (Germany), the estimated performance in terms of the solar fraction could reach up to 43%. However, the monitoring data under realistic operation conditions showed that only a solar fraction between 21% and 33% could be reached [22]. A higher estimated solar fraction value has not been reached due to several issues that comprise higher heating demand compared to the excepted, higher thermal losses in the seasonal storage, and lower solar collector and heat exchanger efficiencies [23]. The same issue has been noticed in other SDHS installed in Neckarsulm and Rostock [24]. Moreover, in the installed plants in Steinfurt-Borghorst, Hamburg, and Neckarsulm II, a considerable deviation between the design and monitored performance due to the high thermal losses in the seasonal and other tanks, high net return temperature, and smaller solar collector area than the planned [25]. The most famous solar community is the Drake Landing Solar Community in Canada. This plant has been able to cover 98% of the space heating demand through solar energy [26]. However, a high-performance variation faces this solar community during a five year of monitoring. According to ASHRAE report [27], the reason behind this underperformance of the system compared to the simulation results is the high thermal losses throughout the network, the storage tank stratification, and pump control. Other than the problems mentioned above, Weissmann et al. [28] stated that the building orientation and the thermal collector orientation combined with the pipe leakages could adversely affect the SHDS performance.

In order to expand the benefits of SDHS, the optimal designing and sizing of SDHS and their relative relevant components (e.g., charging/discharging devices) should be adequately planned [29]. Substantially, planning and construction of large-scale SDHS coupled with seasonal TES is a complex process. Furthermore, the vast options of seasonal TES combined evolve the optimization approach as a viable option to obtain the optimal design and operation conditions of SDHS. The formulation of the optimization problem has two main approaches, the first is to use equation-oriented approach, which leads to non-convex mixed-integer non-linear programming (MINLP) and it can be solved through software packages (e.g., GAMS, MATLAB, etc.) [30]. According to Klatt and Marquardt [31], however, MINLP is still not a suitable method for reasonably sized models. Therefore, MINLP models are often reformulated and solved using mixed-integer linear programming (MILP). This approach relies on simpler and less accurate methods. In this context, Buoro et al. [32] and Welsch et al. [33] formulated a MILP for optimizing SDHS together with conventional power units to emphasize on the renewable energies rule in the residential sector. On the other hand, the second approach refers to the sequential models which rely on detailed equations with accurate results [34]. Therefore, this approach is used in commercial software (e.g., TRNSYS, EnergyPlus, etc.). In this context, Tian et al. [21] and Rehman et al. [35] set up a TRNSYS-GenOpt model to optimize the key design parameters of a SDHS in a multi-objective optimization (MOO) framework. Their results approve the techno-economic feasibility of district heat networks in Nordic climates. Lined up with the environmental benefits of SDHS, Tulus et al. [36] proposed a framework to optimize SDHS design parameters according to economic and environmental indicators based on a generic

optimization tool combined with TRNSYS. Even though the sequential models have great potential in developing validated models [37], the optimization based on sequential models (Heuristics optimization) is computationally costly and have many limitations regarding the optimization process to consider several decision variables comprises the operation, configuration, and sizing of the SDHS in the same framework. Moreover, these Heuristics optimization frameworks failed in considering the stochastic nature of renewable energy sources [38]. In this context, several studies performed a sensitivity analysis in order to investigate the contribution of various parameters to the SDHS model output [38,39]. However, due to the high computational expenses of the Heuristics optimization problems, the most common approach is the Local Sensitivity Analysis (LSA), where the importance of the parameters is investigated by varying one parameter at a time whereas the remain parameters are fixed [40]. This approach is an inadequate practice to cover the input parameters domain and its interactions. Alternatively, the Global Sensitivity Analysis (GSA) approach solve these drawback, where it can offer better coverage for the parameter design space and its relative interactions [41], but it required thousands of simulations in order to cover the design parameters domain sufficiently which does not fit with the Heuristics optimization approach.

This computational obstacle of SDHS simulation may be overcome by using the surrogate model (metamodel) [42]. The metamodel is a generated model of the sequential model, which is typically fast compared to the original detailed model. One of the most widely used metamodel technique is artificial neural networks (ANN) to solve complex engineering problems [43]. The main advantage of ANN is to replicate the detailed model through approximate an implicit relationship based on the training data. In the SDHS context, Yaïci and Entchev [44] utilized ANN to predict the yearly performance of SDHS that covers the domestic hot water and space heating demand in a residential application. While Xia et al. [45] combined the ANN model with a genetic algorithm to optimize the performance of SDHS in a multi-objective framework. Despite the ANN potential in developing accurate metamodels, the generation of an adequate training set required large simulation number. Moreover, the large set of tuning parameters in the ANN model combined with the requirement of large simulation for generating an adequate training set represents a significant limitation in using ANN [46].

All the performance, modeling, economical and legal barriers promote a high variation in quantifying the SDHS benefits over its lifetime [38,47], especially in different community size [48]. Thus, this study aims to propose a methodology framework to address these shortcomings via the following contributions:

1. To develop a robust approach for establishing an ANN model that covers the drawbacks associated with the surrogate modeling technique.
2. To integrate this robust ANN model to solve the computational obstacle associated with heuristics optimization models for SDHS in a MOO framework.
3. To trace the technical failure of the seasonal TES through expanding the decision variables by presenting its geometry and construction design parameters in the optimization problem due to its potential importance, as reported in several established projects [22,24].
4. To examine the community size effect on the performance of the SDHS in a techno-economic optimization framework with consideration for its environmental impact.
5. To investigate the uncertainty using the GSA approach for the economic parameters (investment costs, energy carrier prices, etc.) through taking advantage of the low computational cost feature associated with the robust ANN model.

Hence, the main novelty of the work is to develop a sustainable pathway to trace the techno-economic failures of the SDHS in the residential communities with consideration for its environmental impact. This path is implemented through developing a complete methodological optimization framework based on a robust ANN to showcase the full system potential throughout its lifetime when introduced in different urban community sizes. Moreover, another novelty of this paper is the integration of Global Sensitivity Analysis (GSA) with the Heuristics optimization frameworks; it is the first effort to bridge the heuristics optimization approach and the uncertainty associated with the SDHS design from a global perspective. In this context, the framework starts with developing a detailed simulation for the SDHS based on TRNSYS 18 software [49], the model includes seasonal and short term storages to fulfill both energy demands for the space heating (SH) and the domestic hot water (DHW). The developed TRNSYS model is combined with MATLAB to develop the robust surrogate model and then introduced in a multi-objective optimization problem that comprises the community size effect and the seasonal TES design parameters under two main different optimization settings. The first optimization setting considers only the SDHS equipment sizes, whereas the other setting includes the SST construction materials in the optimization problem. The developed framework can serve as a supportive decision-making tool that assesses the potential of SDHS in Europe and subsequently, accelerating the clean energy transition with promoting a clear statement regarding the new clean energy for all Europeans packages.

2. System description

The study is performed for a virtual residential community with a dedicated solar-assisted district network. The SDHS is modelled in a dynamic simulation software TRNSYS 18, which is introduced earlier in [38]. The main components of the SDHS are the solar collector field, the seasonal storage tank (SST), and the DHW storage tank (DHWT). The solar collector field can be either installed in the residential community roofs or the ground nearby the storages and its relative distribution systems. The SST is a large-scale sensible water insulated reservoir, which is usually half-buried, and it is mainly utilized to accumulate energy for an extended period. The SST is able to cover the SH demand during the winter season through the stored energy during the summer season. On the contrary, the DHWT is relatively a small water TES tank dedicated to supply energy on a daily bases to cover the DHW demand at a temperature of 60 °C. The mismatch between the supply and the customer demand in a daily or seasonal base is covered by auxiliary natural gas heaters. A schematic representation for the analysed SDHS in this work, and its main inputs/outputs are shown in Fig. 1.

The proposed SDHS is divided into three primary circuits; these circuits comprise the solar field circuit, the SH distribution circuit, and the DHW distribution circuit. The solar collector field (COL) is connected to the short- and long-term storages through heat exchangers (HE_1) and (HE_2). These heat exchangers impulse the captured heat through the solar collector to the SH distribution circuit or DHW distribution circuit based on the selected control mode using the Y-type valves. The blue line shows the heat flows in the cold side of the SHDS, whereas the red line represents the hot side, as illustrated in Fig. 1.

2.1. Control system description

The control strategy is designed to maximize the solar contribution where solar energy is utilized to meet the SH and DHW demand. In the DHW operation mode (priority 1), the COL output temperature and the average DHW temperature are the monitoring variables. When this mode is activated, the centrifugal pumps P_1 and P_4 are triggered to transfer the accumulated solar heat to the DHWT through the HE_2. An auxiliary heater using natural gas AUX_2 is installed to cover any shortage in the DHW network supply. Two Y-valves are installed to regulate the water temperature at the DHW distribution circuit by mixing the hot water from the AUX_2 with fresh water from the mainstream.

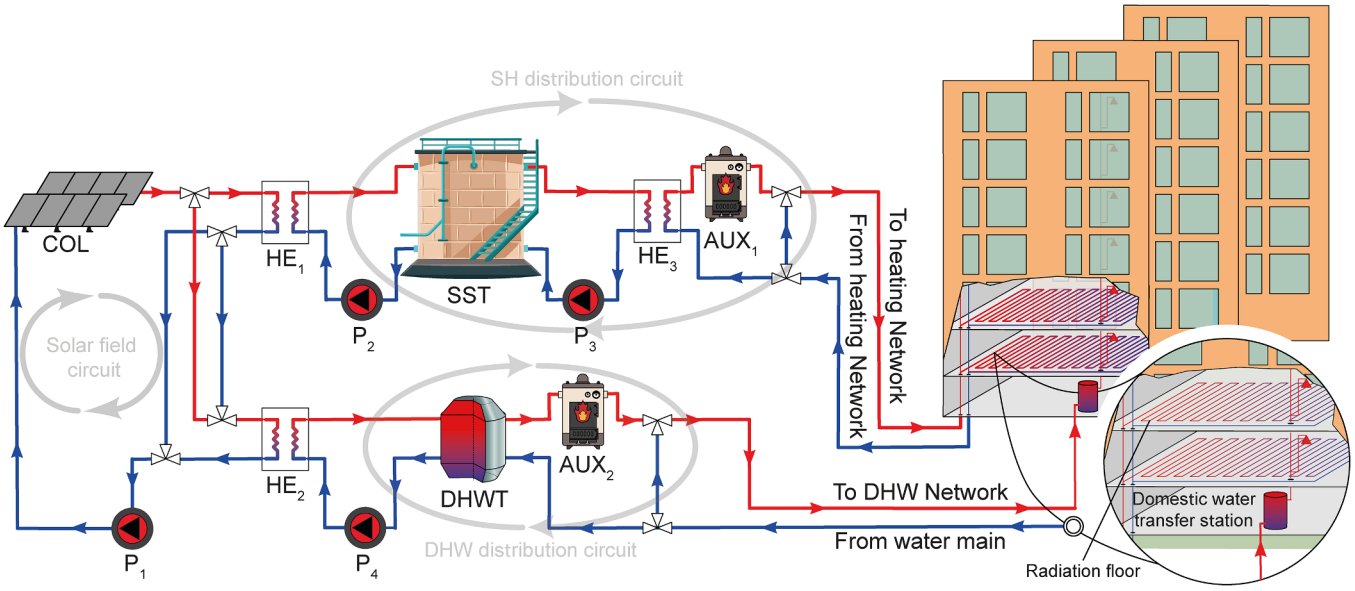

Fig. 1. Simple schematic representation for the SDHS.

In the SH operation mode (priority 2), the COL output temperature, the average DHW temperature, and the temperature at the bottom of the SST are the monitoring variables. When the temperature in the DHWT achieved its set point, and the temperature in the COL is higher than the SST bottom temperature, the SH operation mode is activated. In this mode, pump P_1 and P_2 allow the heat transfer from the solar collector field to the SST through the HE_1. During the demand periods, P_3 impulse the hot water from the bottom of the SST to the SH network through HE_3. Downstream this heat exchanger, a natural gas boiler AUX_1 is installed to cover any failure of the solar system.

In addition to these two control strategies, the simultaneous SH and DHW operation mode (priority 3) is activated when both the previous two modes of control are satisfied. Beside these control operation modes, control loops are developed to regulate the Y-type values in the SH and DHW distribution circuits in order to maintain the set-point temperature at the heating and DHW network.

3. Methodology framework

The proposed methodology framework for the sustainable assessment of the SHDS is outlined in Fig. 2. The first step in the framework is the simulation for the SDHS process through a commercial simulator (TRNSYS 18). Then defining the suitable decision variables range and their relative output, which reflect the thermal performance of the SDHS. Once the decision variables are set, MATLAB creates scenarios based on the decision variables range to cover the process feasibility

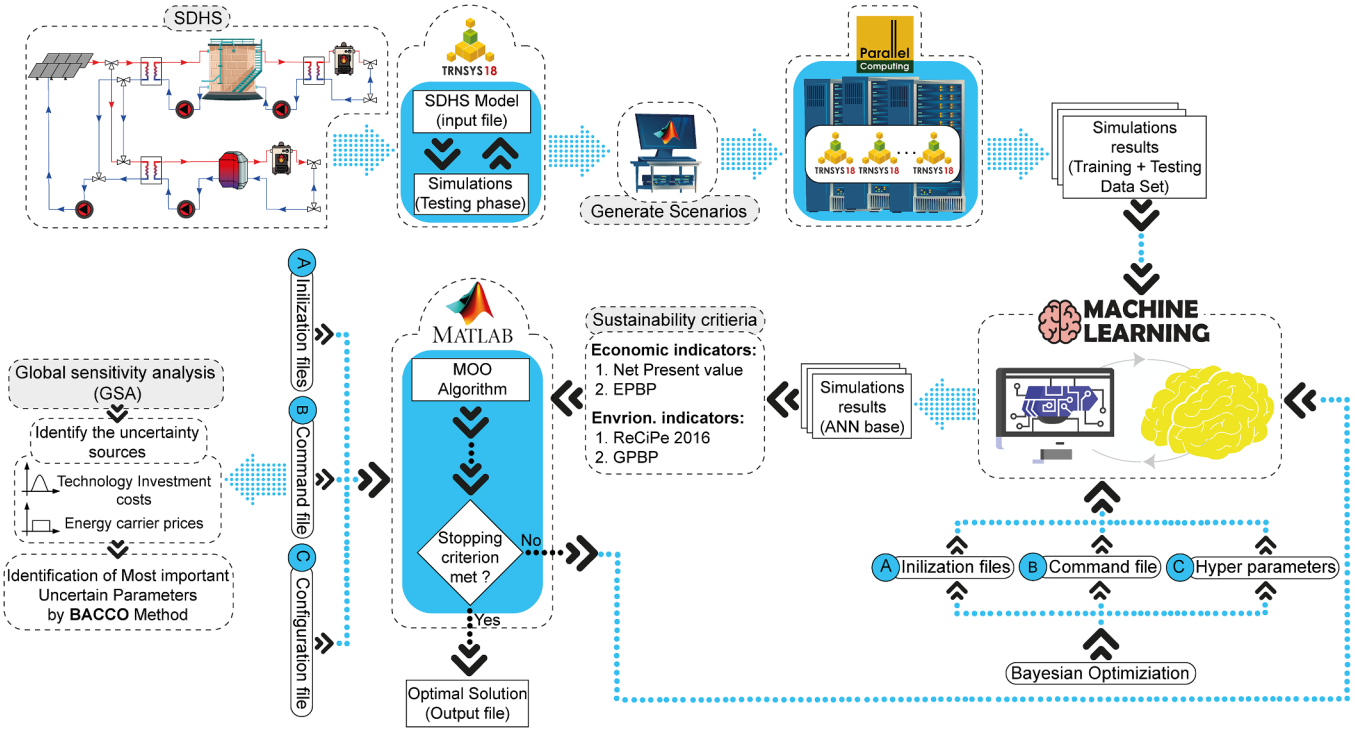

Fig. 2. Sustainable framework for the optimal design of SDHS.

and automatically launches TRNSYS in a parallel manner to simulate these scenarios. With computationally demanding processes, the machine learning approach based on ANN is utilized to alleviate the computationally effort during the optimization phase. Before the MOO stage, the ANN model is coupled with the Bayesian optimization approach to develop a robust ANN model-independent on its tuning parameters (Hyperparameter). To solve the MOO problem, a multi-objective genetic algorithm (MOGA) is introduced to quantify the economic and environmental benefits of the SHDS in the different community sizes, and it is coupled with the developed ANN model. Once the Pareto frontier is generated based on the objective functions, the GSA is presented to illustrate the significant impacts of uncertainty on the economic and environmental indicators [41,50].

3.1. Energy system modelling

The developed SDHS simulation model is built based on TRNSYS18, following the models previously developed by Guadalfajara et al. [51] and Tulus et al. [36]. This software mainly solves the partial differential equations, mainly apply the mass and energy balances equations within the SDHS boundaries. The dynamic nature of TRNSYS simulation environmental assists in introducing the simulation of SHDS more realistically. Aligning with the simplicity idea in calculations, a typical year of operation based on hourly timescale is introduced and then extrapolated in order to show the performance of the system throughout its lifetime with assuming the same climatic conditions and demands over the years of operation.

A part of the methodology framework is to tackle the technical failure of the SDHS comprising the construction, sizing, and operation of its equipment when introduced in various community sizes. Thus, being the solar collector, storages tanks are the key decision variables in designing an optimal SDHS [36], 15 decision variables including the orientation of solar collectors and the construction and sizing of the storage tanks are introduced in the optimization problem. For each simulation, 19 aggregated outputs are considered; these outputs comprise the energy production in the solar field, the energy stored in the storage tanks, the supplied energy by the auxiliary heaters, and the energy consumption by the pumps.

3.2. Robust ANN solution procedure

As stated in the introduction, some barriers limit the using of the ANN. Aligning with these drawbacks, this section explains the approach carried out in this study to develop a robust metamodel that eliminates them. The proposed methodology starts with the data generation (known as sampling) in which a vast range of training points are introduced to testify the metamodels accuracy converges and its time consumption. The Bayesian optimization approach is then combined with the sensitivity analysis to test the variety of the metamodel settings. Once the metamodel settings are nominated, the ANN model is developed with testing the balance between the model accuracy and the time consumption.

3.2.1. General background on ANN modeling

The ANN is a supervised learning technique which covers a board range of models and learning algorithm. This study is mainly focussed on the feedforward neural network with multi hidden layers. Generally, the neural network consists of several hidden layers where each layer consists of several neurons; these neurons propagate information using weighted connections and transfer functions. The number of neurons in the input and output layers is equal to the number of the model input and output, respectively. Since the number of hidden layers and their relative neurons selection increase the overfitting risk, the hidden layers are interpreted based on an optimization algorithm that can be used to interpret other ANN settings [52].

In addition to the hidden layers and its relative neurons, the ANN architecture is also defined through other settings comprising the training/learning method, the activation functions, momentum mean, and the learning rate. Thus, the neural network is based on investigating the optimal setting for the hyperparameters number of the hidden layers, number of neurons in the hidden layer, training function, activation function-hidden layer, activation function- output layer, learning rate, and momentum mean.

3.2.2. Data generation and preparation

The process of building the training data for the surrogate model is known as sampling. The performance of the surrogate mainly depends on the quality of the sampling strategy as well as its size. In order to maintain the quality of the surrogate model without high computational cost, the sampling strategy represents significant importance [53].

The sampling strategy can rely on the grid pattern where this sampling method is derived from the design of experiment literature (factorial, Box-Behnken designs), space-filling design (Latin hypercube design, low-discrepancy sequences), and sequential sampling approach where the samples are generated adaptively where information is required [54]. In this context, the low-discrepancy sequences (Sobol's LP_{τ}) are utilized to create the training data since it is assumed to cover the space design domain more efficiently in comparison to the Latin hypercube design [55]. The generation process starts with generating N samples in an n-dimensional unit where n represents the number of decision variables. Then the generated points turned into $n \times N$ input matrix where each row represents a set of decision variables to obtain the thermal performance of SDHS. The data generation process is built automatically in MATLAB and connected to TRNSYS to perform the required simulations in a parallel manner.

The appropriate sampling size mainly depends on the size of decision variables along with the computational budget. At some points, increasing the size of samples has a negative effect on improving the performance of the surrogate model with an excessive computational cost. Thus, aligning with building a surrogate model independently on the sampling size at a suitable computational cost, the metamodel is trained using different sample sizes in a range between 32 and 8192, which is within our acceptable computational limits (10,000 simulations). In the process of the ANN model setting selection, the k-fold cross-validation process is presented in order to avoid the overfitting issue [56]. This process involves splitting the generated samples into k subsets, where each subset includes an equal set of samples. The ANN model is trained on k-1 subsets and tested on the remain k subset. The process is repeated k times. Thus, each k subset will be used as a testing set.

3.2.3. Assessing model setting and convergence

The robust surrogate model building process has been divided into two main steps; the model setting selection and the model convergence testing, as shown in Table 1. In the first step, model settings and its

Table 1
Building the Robust ANN model steps.

Investigation	Model settings	Convergence
Training sets	64, 256, 1024	32, 64, 128, 256, 512, 1024, 2048, 4096, 8192
Purpose	To find suitable model settings	To assess model accuracy in balance with its computing time

relative hyperparameters through using the Bayesian optimization approach at different training set sizes are emphasized. The optimization approach is combined with the sensitivity analysis to estimate the importance of the hyperparameters. In the second step, the convergence of the ANN model is assessed through testing the develop a surrogate model based on the optimal model settings under a wide range of training set to define the optimal sample size.

Corresponding to the importance of tuning the ANN model hyperparameters in determining the model accuracy, different approaches, including the naive gird search and random search can be utilized in this context. However, these approaches exhaustively time-consuming; thus, limited decision variables can be investigated based on these methods [57]. In addition to these approaches, the optimization workflow can succeed in solving the drawbacks associated with the traditional methods. In this regard, a few generic optimization algorithms, including genetic and particle swarm algorithms, have been applied to optimize the metamodels hyperparameters [58,59]. However, these algorithms have dimensionality problems [60]. Among these approaches, the Bayesian optimization algorithm demonstrates better performance in several cases [61].

In our case, it is applied due to its beneficial advantage in solving computationally intensive cases since it can include binary, continuous, and discrete hyperparameters in the optimization problem [62]. Moreover, the Bayesian hyperparameter optimization algorithm is capable of handling the optimization problem in parallel computing manner using a cluster of computers [63]. This approach aims to constructs a probabilistic model using the Gaussian process, which is updated with each new observation and has a definitive goal of improving the metamodel accuracy. Table 2 lists the hyperparameters settings options in the two stages of the development of the Robust ANN model in comparison to the default setting of the ANN.

In addition to the hypermeters tuning through using the Bayesian optimization algorithm. A sensitivity analysis based on screening design is attractive to eliminate irrelative hyperparameters from the second stage (B. Convergence). Often fractional factorial designs with resolution III or IV are introduced in the early stages of screening designs. However, these design types required a broad set of runs and have no capability of capturing the quadratic terms [64]. Thus, using the definitive screening design proposes efficient properties in minimizing the number of the required runs, and estimating the quadratic terms. The evaluation of the definitive screening design is conducted through ANOVA, where a Pareto chart is constructed to rank the significant hyperparameters [65].

When the least significant hyperparameters are identified through the definitive screening design, an interactive parallel coordinate plot is presented. This plot is then combined with histograms for each hypermeter showing its setting distribution in providing an accurate metamodel.

In order to characterize the performance of the developed metamodels, a group of metamodel performance metric are utilized to evaluate its accuracy. These metrics include three standard evaluation measures; (i) adjusted R-squared ($R^2 - Adj.$), (ii) Coefficient of Variation ($C.V$), and (iii) Symmetric mean absolute percentage error ($SMAPE$), their formulas are expressed in Eqs. (2)–(4).

$$R^2 = 1 - \frac{\sum_{i=1}^{n} (y_{predict,i} - y_{data,i})^2}{\sum_{i=1}^{n} (y_{data,i} - \bar{y}_{data})^2} \tag{1}$$

$$Adjusted - R^2 = 1 - \frac{(1 - R^2)(n-1)}{n-k-1} \tag{2}$$

$$CV(\%) = \sqrt{\frac{\sum_{i=1}^{n} (y_{predict,i} - y_{data,i})^2}{\bar{y}_{data}}} \times 100 \tag{3}$$

$$SMAPE(\%) = \frac{1}{n} \sum_{t=1}^{n} \frac{|y_{data} - y_{predict}|}{|y_{predict}| + |y_{data}|/2} \times 100 \tag{4}$$

where $y_{predict,i}$ is the predicted value at time point i, $y_{data,i}$ is the actual data at time point i, n is the sample size, and k is the number of regressors. Following the proposed standard accuracy evaluators. The CV is used as an objective function in the model setting stage for two main reasons. First, it's recommended by ASHRAE for evaluating the energy systems. Second, it's a normalized value, which can be more convenient for comparison purposes [66].

3.3. Sustainable assessment

The developed framework evaluates the proposed SHDS based on three main criteria comprise: the technical performance with details regarding the construction and operation of the equipment in the proposed plant, as well as the economic and environmental performance throughout the system lifetime.

3.3.1. Technical assessment

The technical analysis of the SHDS, coupled with sensible seasonal TES in the proposed framework, can be implemented in two main stages. The first stage examines the thermal performance of the sensible seasonal TES based on the storage dimension and its construction materials. While the second stage proposes several indicators to assess the overall performance of the SDHS.

Within the SST analysis, a large water cylindrical tank built over the ground and filled with water to serve as a seasonal storage unit in the SHDS is investigated. The SST constructed based on reinforced concrete and insulation from the top, side, and bottom based on various insulation material to reduce its heat loss to the environment. The SST characterization is evaluated based on the storage heat capacity and heat loss during its operation [67]. The energy provided by the fully stratified SST can be expressed, as shown in Eq. (5):

$$Q_{SST} = \int_0^t \dot{m}_{SH} C_p \Delta T_{SST} \tag{5}$$

where $\dot{m}_{SH}$ is the water mass flow rate in the SH distribution circuit, C_P is the specific heat, and ΔT_{SST} is a temperature difference between the

Table 2
The model setting in the two stages of developing a Robust ANN model.

Model setting (hyperparameter)	Model settings	Convergence	Default
1. Number of the hidden layers	1:10	3	1
2. Number of neurons	1:50	14	10
3. Training function	a. Levenberg Marquardt b. Bayesian regularization c. Scaled conjugate gradient d. Resilient backpropagation	b	a
4. Activation function, hidden layer	i. logsig, ii. tansig, iii. purelin	i	ii
5. Activation function, output layer	i. satlin, ii. logsig, iii. tansig, iv. purelin	iv	iv
6. Learning rate	0.001:0.5	0.001	0.01
7. Momentum mean	0.001:1	0.004	0.9

extracted and replaced water from the storage tank to cover SH demand.

Another characterization key of the SST performance is the thermal heat losses, and it can be evaluated based on heat losses through the top (U_{Roof}), sideways (U_{Wall}), and bottom of the storage (U_{Gnd}). The thermal heat loss through these surfaces depends on the construction material, the insulation material, the ground properties, and the height to diameter ratio [68], A set of a nominal performance metric is introduced to evaluate the technical performance of the solar field circuit, and SH and DHW distribution circuits. These indicators comprise the solar collector, SST, and DHWT efficiencies [69,70], and the annual solar fraction for both the SH and DHW distribution circuits [71,72]. These performance indicators are calculated using Eqs. (9)–(13) as a function of the energy flow over the solar field and the distribution circuits:

$$\eta_{COL} = \frac{\int_0^t \dot{Q}_{Useful}}{\int_0^t \dot{Q}_{SOL}} \tag{6}$$

$$\eta_{SST} = 1 - \frac{\int_0^t \dot{Q}_{SST\ loss}}{\int_0^t \dot{Q}_{HE_1}} \tag{7}$$

$$\eta_{DHWT} = 1 - \frac{\int_0^t \dot{Q}_{DHW\ loss}}{\int_0^t \dot{Q}_{HE_3}} \tag{8}$$

$$S.\ F_{SH} = 1 - \frac{\int_0^t \dot{Q}_{AUX_1}}{Q_{SH\ load}} \tag{9}$$

$$S.\ F_{DHW} = 1 - \frac{\int_0^t \dot{Q}_{AUX_2}}{Q_{DHW\ load}} \tag{10}$$

where $\dot{Q}_{Useful}$ and $\dot{Q}_{SOL}$ are the useful energy produced and received by the solar collector field, respectively. $\dot{Q}_{SST\ loss}$ and $\dot{Q}_{DHW\ loss}$ represent the heat loss in the SST and DHWT, whereas the $\dot{Q}_{HE_1}$ and $\dot{Q}_{HE_3}$ are the heat transfer rate through the heat exchangers HE_1 and HE_3. Moreover, $\dot{Q}_{AUX_1}$ and $\dot{Q}_{AUX_2}$ states for the auxiliary energy rate provided by the natural gas boilers in the SH and DHW distribution circuits to cover the SH load ($Q_{SH\ load}$) and DHW load ($Q_{DHW\ load}$) demand when the solar system fails in reaching the set temperature point.

3.3.2. Economic assessment

In the current study, the economic performance of the system configuration is implemented through the life cycle costing (LCC) methodology [73,74].

The LCC approach is a valuable technique for assessing the economic performance of the energy system in terms of the initial investment cost combined with its operational and replacement cost throughout the system lifetime. The LCC approach assists the decision-makers in comprehensively interpreting the energy system's economic performance throughout its life cycle and subsequently avoiding extra expenses in the early stages of design even though additional investment cost is required [75].

The main principle of the LCC methodology is the future system value, where all system expenses throughout its lifetime are discounted to its present value. The total present value (NPC) can be estimated by considering the initial investment cost (C_C), the operational cost (C_O), and the replacement cost (C_R):

$$NPC = C_C + C_O + C_R \tag{11}$$

The initial investment cost states for the initial capital cost at the project starting point. It considers the equipment cost, installation, and transportation cost. In addition to any possible contingency expenses, and it can be expressed as follows:

$$C_C = (1 + \alpha_{CF}) \sum_k (PCE_k.\ FBM_k) \tag{12}$$

where PCE_k represents the initial capital cost of purchased unit k, FBM_k is the bare module factor, which states for the installation and transportation cost of unit k, and α_{CF} donates for the contingency factor.

PCE_k fetched the initial purchased cost from the base year (year A) to the year of installation (year B) based on the Chemical Engineering Plant Cost Index (CEPCI) using the following equation:

$$PEC_k = PEC_k^{yearA} \frac{CEPCI^{\ year\ B}}{CEPCI^{\ year\ A}} \quad \forall\ k \tag{13}$$

The initial purchased cost of unit k at year A can be estimated using Eqs. (14)–(17):

$$PEC_k^{yearA} = \alpha_k CAP_k^{\beta_k} \quad \forall\ k = COL, DHW, AUX \tag{14}$$

$$PEC_k^{yearA} = CAP_k^{\beta_k}.\ 10^{[\alpha_k (\log_{10} CAP_k)^{\beta_k}]} \quad \forall\ k = HE_1, HE_2, HE_3 \tag{15}$$

$$PEC_k^{yearA} = \alpha_k ln\left(\frac{CAP_k}{1000}\right) + \beta_k \quad \forall\ k = P_1, P_2, P_3 \tag{16}$$

$$PEC_k^{yearA} = Ins_{SST} + Con_{SST} \quad \forall\ k = SST \tag{17}$$

where

$$Ins_{SST} = \alpha_k CAP_k^{\beta_k} \quad \forall\ k = XPS, MW, FG \tag{17.1}$$

$$Con_{SST} = \alpha_k CAP_k^{\beta_k} \quad \forall\ k = NC, HPC \tag{17.2}$$

$$Con_{SST} = \alpha_k e^{\left(\frac{\beta_k}{10^5} CAP_k\right)} \quad \forall\ k = UHPC \tag{17.3}$$

where α_k and β_k are the equipment or material purchase cost parameters, CAP_k is the design variables of equipment k. The design variables are the solar collector field area (A_{COL}), the storage tank volume (V_{SST}, V_{DHW}), the SST insulation type (XPS, MW, FG) comprising extruded polystyrene, mineral wool, and foam glass gravel, respectively, the construction material type (NC, HPC, $UHPC$) comprising Normal concrete, high performance concrete, and ultra-high performance concrete, respectively, the heat exchanger areas (HE_1, HE_2, HE_3), and the pumps discharge mass flow rates ($\dot{m}_1$, $\dot{m}_2$, $\dot{m}_3$, $\dot{m}_4$).

The operational cost states for the annual maintenance cost of different equipment, the electricity consumption by the centrifugal pumps, and energy consumption by the natural gas auxiliary heaters. It can be expressed as follows:

$$C_O = C_M PWF_M + C_P PWF_P + C_{AUX} PWF_{AUX} \tag{18}$$

where the C_M, C_P, and C_{AUX} donate for the annual maintenance cost, the recirculation pumps, and the auxiliary heater consumption cost. While PWF tends for the time value of the money with consideration for the inflation rate (i) and discount rate (d) throughout the proposed system lifetime.

The replacement cost counts for the depreciation associated with several equipment during the lifetime of the SDHS. This equipment is the solar collector field, the DHW storage tank, the heat exchangers, and the auxiliary heaters. The replacement cost can be calculated using Eq. (19) with consideration for the equipment present value:

$$C_R = PVF_n \sum_k (PEC_k.\ FMB_k) \tag{19}$$

where PVF_n is the present value factor of future cash flow at year n.

The economic viability of the SDHS can be specified as well based on the economic payback period ($EPBP$) [76]. It is widely used for evaluating energy system performance throughout its lifetime, and it's usually expressed in years. The shorter the payback period, the more favourably a project is ensured. The computation of the ($EPBP$) can be obtained by dividing the future system value (NPC) by the yearly cost saving for using the SDHS as follows:

$$EPBP = \frac{NPC}{Annual\ \ cost\ \ saving} \tag{20}$$

3.3.3. Environmental assessment

In addition to the LCC approach for assessing the economic performance of the SHDS. The system environmental impact is evaluated using a life cycle assessment approach (LCA) [77]. This approach empowers a comprehensive analysis of the system components during its production as well as their operation and disposal based on the "cradle to grave" concept [78]. The LCA, as standardized in the ISO 14040 series [79–81] comprises several phases that trail a specific sequence; the goal and the scope definition, life cycle inventory, and impact assessment.

The LCA conducted within this study proposes the goal and scope stage for defining the system boundary and its functional unit. In this context, the functional unit was defined as the annual heating demand for the SH and DHW over the system time horizon. The SDHS boundary is drawn based on the "cradle to gate" concept since this study focus on the existing district heating with excluding the disposal phase (end of life). This is a common practice in the LCA approach as the disposal phase is negligible compared to the production and use phases. Moreover, the recycling phase is insignificant as well due to its advance and difficulty in prediction [33].

In the life cycle inventory and impact assessment stage, based on several databases, the material input, output, and their relative energy consumption are compiled during the construction and operation of the plant. In the current study, the impact of equipment manufacturing, as well as the utility energy consumption (natural gas by electricity) by the SHDS, are considered throughout the whole lifetime. Furthermore, the material transportation to the site as well as the plant components impact during its operation is also considered. These impact data are retrieved from the Ecoinvent 3.5 database [82].

Afterwards, the inventory data are weighted and translated into impact categories. These damages comprise; the damage to human health, the damage to the ecological system, and resources damage. In this work, the ReCiPe 2016 framework is promoted to evaluate different environmental categories based on the aggregated endpoint indicator metric (*RCP*) rather than using the mid-point indicators, which would be misleading in interpreting the overall SDHS environmental performance with different sized systems. The *RCP* can be expressed as follows:

$$RCP = \sum_{d} \delta_d \varepsilon_f DAM_d \quad \forall\ d \tag{21}$$

where DAM_d represents the endpoint of the damage category d, and δ_d, ε_d are the specific normalization and weighting factors. The normalized factors are specified based on the damage to the European land uses, and their relative material extractions [83]. On the other hand, the weighting factors are estimated based on the ReCiPe 2016 recommendation [38].

In addition to the LCA indicator, the greenhouse gas payback period (*GPBP*) is used to measure the system sustainability of the system [84]. Even though the SDHS is almost a free greenhouse gas emissions during its operation, the environmental damage of such this system is generated during the production and disposal processes [85]. The (*GPBP*) is defined as the environmental impact reduction potential as a result of the SDHS installation, and it can be expressed as follows:

$$GPBP = \frac{RCP}{Annual\ \ RCP\ \ saving} \tag{22}$$

3.4. Optimization problem

This stage focusses on solving the computational obstacle associated with heuristics optimization models through using the developed robust ANN model in a MOO problem. Moreover, it tends to trace the technical failure of the SDHS through expanding its decision variables by presenting the SST geometry and construction design parameters as well in an optimization framework. Therefore, the energy performance is optimized to cooperate with the economic and environmental system requirements using the MOO framework to deal with the multi-objective conflict nature. Lastly, the community size effect on the performance of the SDHS was examined in separate optimization problems.

In the solar district heating system, the formulation of an optimization problem always deals with the conflicting nature associated with such these energy systems. Therefore, researches are often concern about the technical performance aligning with its economic profiles [23,35]. In this study, we add more real-world nature objective by considering the environmental impact in the problem formulation. Therefore, the current study emphasis on optimizing the LCC of the SHDS presented by the total plant cost (*NPC*) simultaneously with the LCA presented the eco-points (*RCP*) to satisfy the technical requirement, and it is given as:

$$\min\{f_1(x), f_2(x)\}$$

$$s.\ t. \quad h(x) = 0 \quad g(x) \geq 0$$

$$lb_i \leq x_i \leq ub_i \quad i \in \{1, \cdots, 15\} \tag{23}$$

where f_1 is the plant net present value (*NPC*) and f_2 is the ReCiPe 2016 aggregated impact factor (*RCP*), h donates for the equality constraints, which corresponding to the mass and energy balance equation solved implicitly in TRNSYS in the first stage. While g donates for the inequality constraints, which correspond to the correct technical performance of SDHS. These constraints must maintain the annual solar collector efficiency above 60%, whereas SH annual solar fraction and SST efficiency should be maintained above 50% based on Bauer et al. [22] and Solites [86] recommendations.

The optimized solution in the multi-objective problem provides a set of non-dominated solutions (Pareto frontier points), which represent optimal trade-off solutions between the economic and environmental objectives that satisfy the technical performance constraints. The extreme points in the Pareto frontier called the anchor points, and it corresponds to the minimum economic and environmental impact solutions. In the MOO problems using the classical methods based on point by point approach (weighted sum or the ε-constraint method) [87], the optimization outcome represents a single optimized solution based on a particular search direction, which often delivers local information (suboptimal solution). Furthermore, due to the dependency of the optimal solutions on the initial chosen solution, these approaches fail in solving different optimization problems type [88]. Aligning with these limitations, an evolutionary approach based on a technique called Pareto-ranking [89] is utilized to estimate approximate Pareto-optimal solutions based on the (*NPC*) and (*RCP*) objective functions.

The SDHS performance is examined in four different community sizes (10, 25, 50, and 100) based on 15 decision variables; these decision variables describe various components in the SDHS, including its sizing as well its relative orientation and construction. These variables can be categorized based on the circuit name. In the solar field circuit, (i) COL area (A_{COL}), (ii) COL inclination angle (β_{COL}), and (iii) number of COL in series (N_{COL}) are considered. In the SH distribution circuit, (i) SST volume (V_{SST}), (ii) SST aspect ratio (HDR), (iii) SST construction material (λ_{con}), (iv) SST roof, wall, and ground insulation material type (λ_{ins}), (v) ground insulation material type ($\lambda_{ins\ gnd}$), (vi) roof, wall, and ground insulation material thickness (T_{Roof}), (T_{Wall}), and (T_{Gnd}), respectively, and (vii) AUX_1 fraction (FC_{AUX1}) are considered. Finally, in the DHW distribution circuit, (i) DHWT volume (V_{DHWT}), (ii) DHWT aspect ratio (HDR_{DHW}), and (iii) AUX_2 fraction (FC_{AUX2}) are considered. A wide range of these decision variables is estimated for simulation and optimization processes based on real implemented projects in EU and recommendation for various articles, as shown in Table 3. On the other hand, the sizing of other equipment units in the SDHS is determined through mathematical equations that relate them to the decision variables.

In the current framework, the Multi-Objective Genetic Algorithm

Table 3
Decision variables for the SHDS categorized by circuit name.

Circuit name	Decision variable	Unit	Uniform	Discrete	Ref.
Solar field circuit	A_{COL}	m^2/MWh/a	0.1:2		[38,90]
	β_{COL}	°	20:70		[48]
	N_{COL}	–	1:5		
SH distribution circuit	V_{SST}	m^3/MWh/a	1:20		[22,91]
	HDR	m/m	0.3:1.5		[68,92]
	d_{Roof}	m	0.2:0.7		
	d_{Wall}	m	0.2:0.7		[93,94]
	d_{Gnd}	M	0.2:0.7		
	λ_{con}	W/m.K	–	*NC* = 1.5 W/m.K *HPC* = 2.5 W/m.K *UHPC* = 1.6 W/m.K	[95,96]
	λ_{ins}	W/m.K	–	*XPS* = 0.032 W/m.K *MW* = 0.04 W/m.K *FG* = 0.06 W/m.K	[97,98]
	$\lambda_{ins\ gnd}$	W/m. K	–	*XPS* = 0.032 W/m.K *MW* = 0.04 W/m.K *FG* = 0.06 W/m.K	
	FC_{AUX1}	%	0.1:1		
DHW distribution circuit	V_{DHWT}	m^3/MWh/a	0.05:0.25		[38,69]
	HDR_{DHWT}	m/m	1:2		[93,99]
	FC_{AUX2}	%	0.1:1		

(MOGA) is introduced, as it can be coupled easily with a simulator, Blackbox models or even models based on algebraic equations. The MOGA is particularly able to handle a set of points simultaneously, which would empower the user to obtain several Pareto frontiers in a single run [30]. An elitist genetic algorithm (a variant of NSGA-II [100]) is nominated. This algorithm can handle a multi-objective problem in a parallel computing manner. Moreover, it can handle discrete and continues variables, along with equality and inequality constraints [101]. Following the evolutionary approach, the solutions are iteratively modified according to the internal ranking of each population. These populations are generated based on the mutation and crossover functions [30]. An automated simulation-based optimization model is performed by combining the generated robust metamodel based on ANN with the NSGA-II algorithm. The MOGA uses the NSGA-II algorithm with 1000 initial population due for 300 generations based on Alajmi et al. [102] recommendation.

3.5. Sensitivity analysis

The final step in the methodology framework is to perform a sensitivity analysis, which is a common approach that offers an insight into the important model parameters. Given the drawbacks in the LSA, the GSA approach based on Bayesian analysis of computer code outputs (BACCO) [103] is employed. The main advantage of this approach is its ability to cover a wide range of uncertain parameters and interactions with consideration for their relative distributions. Furthermore, it offers a substantial computational improvement compared to using expensive GSA based on Monte Carlo simulations [104].

The BACCO method entails two main key stages. In the first step, a statistical representative model (i.e., an emulator) is built based on a set of training data points derived from the developed simulation-based optimization model. The training data are ideally cover the feasible design domain using a multidimensional space-filling algorithm (Latin hypercube design). Prior to the second stage, the cross-validation approach is applied automaticity to estimate the emulator accuracy. The second stage uses the constructed emulator (which is efficient in covering a multidimensional design domain in low computational expenses in comparison to the original optimized model) in quantifying the importance of parameters in interest [105]. The performed sensitivity analysis is presented in terms of the percentage variance contribution of each input with respect to the economic (*NPC*) indicator and environmental indictor (*RCP*).

4. Case study

To better illustrate the capabilities of the proposed framework, the methodology procedure is applied to a SDHS located in Madrid (Spain) to meet the heating demand of different sized neighbourhood community (10, 25, 50, and 100 buildings). Each building comprises 28 apartments with 90 m^2 of useful area [106] per apartment and equipped with a radiant underfloor heating system and a domestic hot water system to meet the SH and DHW demand at 50 °C and 60 °C, respectively. The SDHS model validation and heating demand comparison were implemented in comparison to Guadalfajara et al. [107] and Tulus et al. [38].

For comparison purposes, a base case using only a natural gas boiler is considered. This conventional system is able to fulfil the SH and DHW demand alone independently from the SDHS.

4.1. SDHS model specification

The solar collector field in the SDHS consists of flat-plate collectors (type ARCON HT-SA 28/10) designed for large applications [36]. These collectors are connected in series and oriented toward the south. A 33% mixture of glycol in water (C_p = 3.8 kJ/kg·°C at 50 °C) is initiative as a working fluid in the solar field circuit with a nominal recirculation flow rate of 20 kg/h·m^2. On the other hand, the SH and DHW distribution circuits are operated with water.

The SST is a partially buried tank with a cylindrical section. Since the tank construction is a part of the optimization problem, the seasonal storage design parameters are initialized based on the constructed project in Friedrichshafen (Germany) [96], where normal concrete with

a thickness of 0.5 m was selected as a construction material. For the storage insulation, the mineral wool was placed outside the concrete with a thickness of 0.3 and 0.2 m for the roof, wall, and ground, respectively. On the other hand, the DHW is a relatively small tank compared to the SST since it is utilized for only daily services, the DHWT constructed with an overall heat coefficient of 0.3 W/(m^2·K) [107]. To cover any shortage of the solar system, natural gas boilers with efficiency 93% are utilized as auxiliary heaters for both SH and DHW distribution circuits.

To reproduce the transient behaviour associated with the simulation process, all the TRNSYS simulations were implemented with a time step of 15 min [108]. The system assessment was performed over three years of simulation (28,260 h), and the results after the third year are extrapolated over the SDHS lifetime. The three years of simulation idea is due to the homogeneous assumption inside the SST where SST temperature is equal to 30 °C at the beginning of the first year of simulation. Therefore, after two years of simulations, this initial assumption is eliminated, and the change in temperature becomes insignificant in the following years [23]. According to the United Nations Environment Programme [109], the lifetime of the SDHS is 40 years, where several equipment include the solar collectors, heat exchanger DHWT and auxiliary heaters need to be replaced after only 20 years of operation.

4.2. Climate and demand profiles

The climate data for Madrid is obtained from the EnergyPlus database [110]. These data include the incident solar radiation, ambient temperature, relative humidity, and other relative information. The monthly average ambient temperature and its relative incident solar radiation per solar collector area are shown in Fig. 3.

The space heating demand is established based on the implemented work by Guadalfajara [107] in order to develop a 7-story building that meets the minimum requirement of the Spanish regulations for residential buildings. A 3D building model is developed using SketchUp [111] and imported into TRNSYS, where the occupancy densities and building materials comprising its windows and insulations are defined. By simulating the developed building in TRNSYS, the annual space heating demand profile is generated based on an hourly timescale. The generated SH demand is then extrapolated for the different urban community sizes, and the monthly SH demand is shown in Fig. 3.

On the other hand, to generate the DHW demand for the investigated residential buildings, Tulus et al. [38] was followed, where the DHW demand is based on three main factors: (i) the daily water consumption per person, (ii) monthly water temperature from the public distribution network, and (iii) the number of occupations per household. These data are imported into computer software, DHWcalc [112]. This software can generate a realistic hourly DHW consumption profiles with consideration for main controlling factors, as shown in Fig. 3.

4.3. Economic and environmental input data

The parameters for the initial investment cost are outlined in Table 4. Following Tulus et al. [36], the maintenance cost is estimated to be 1.5% of the initial purchase cost of the equipment. The prices of natural gas and electricity are 0.0526 and 0.1873 Euro/kWh, respectively, based on the EUROSTAT database [113]. Moreover, the inflation rate associated with natural gas and electricity is 5.9% and 5%, respectively [38]. According to Braungardt et al. [114], the inflation rate associated with the proposed system throughout its lifetime is set to be 2.3%, with a discount rate of 3.5%.

The LCA data were retrieved from the Ecoinvent database [82]. This database comprises the damage categories caused by the SDHS main equipment and their relative utilities based on the ReCiPe 2016 methodology (see Table 5).

4.4. Uncertainty characteristics

A correct quantification of the uncertainty is vital to obtain reliable results of the SHDS model. This analysis would support decision-makers in the early design stages. The probabilistic approach, which treats the uncertain parameters as a random variable, is the most common approach to quantify the uncertainty associated with parameters [121]. In the current study, we focus on the economic parameters and their corresponding uncertainty. In total, 13 individual uncertain economic parameters are identified in this study. These parameters are classified into three main categories:

- Investment cost: The solar collector field, the storage, and their relative utilities in the SDHS are considered uncertain since this equipment is a market-driven. Thus, the prices in the early stages of design might differ from the final investment cost [122].
- Economic factors: Aligning with the changes in the energy policies for accelerating the transformation toward clean energies, the economic parameters such as annual inflation rate, market discount, and maintenance factor can change during the long lifetime of SDHS.
- Energy carrier: Normally, the prices of natural gas and electricity are deterministic parameters. However, throughout the system lifetime, the SDHS energy carriers might change due to the market or the energy policies [123].

A summary of the uncertain economic parameters and their characteristic distribution is shown in Table 6.

5. Results and discussion

In the current study, the results are divided into three main parts. The first part offers a deep analysis to build a robust ANN model by comprising the Bayesian optimization approach assisted sensitivity analysis. This part purposes an affordable metamodel that solves the computational obstacle associated with heuristics SDHS model built-in TRNSYS. Then the second part depicts the performance of SDHS in various urban community sizes in an optimization framework using the developed ANN model. This framework intends to tackle the seasonal TES design parameters and its geometry effect to enhance the feasibility of the SDSH in various community sizes. Next, the SDHS optimal design is expressed adequately through including the uncertainty associated with several related economic parameters based on GSA to support the decision-making process.

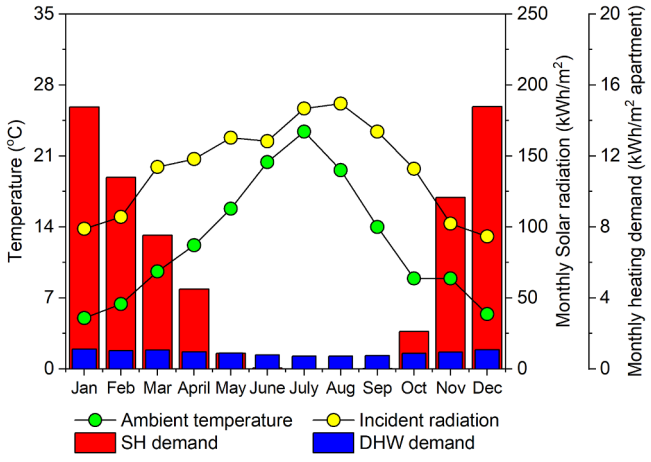

Fig. 3. The climate conditions in Madrid and energy demand per apartment.

Table 4
The economic parameters of SDHS equipment.

Unit	*Options*	α_k	β_k	CAP_k	Range	Base year	*Ref.*	FBM_k
Solar collector		974.2	0.8330	Aperture area (m^2)	4,000–15,000 m^2	2007	[115]	1.00
DHWT		3955	0.6500	Volume (m^3)	1–100,000 m^3	2007	[116]	1.00
Auxiliary heater		225.0	0.7460	Duty (kW)	600–10,000 kW	2001	[36]	2.10
Heat exchanger		3.133	0.3310	Exchange area (m^2)	10–1000 m^2	2001	[36]	3.29
Pump (P_1, P_2)		389.0	283.2	Mass flow rate (kg/h)	15,000–100,000 kg/h	2009	[117]	3.24
Pump (P_3, P_4)		389.0	717.0	Mass flow rate (kg/h)	15,000–100,000 kg/h	2009	[117]	3.24
SST insulation	*XPS*	561.09	0.397	Material thickness (m)	0.05–0.8	2017	[118]	1.00
	MW	1902.7	0.942	Material thickness (m)	0.05–0.8	2018	[119]	1.00
	FG	311.41	0.968	Material thickness (m)	0.05–0.8	2014	[120]	1.00
STT construction	*NC*	4178.1	−0.394	Volume (m^3)	1–100,000 m^3	2000	[97]	1.00
	HPC	2575	−0.363	Volume (m^3)	1–100,000 m^3	2004		1.00
	UHPC	90.83	−3	Volume (m^3)	1–100,000 m^3	2004		1.00

Table 5
Specific ReCiPe 2016 aggregated impact factor for the main SDHS equipment and utilities, in ReCiPe points (Pt) per characteristic dimension [82]

Unit	Option	Impact factor (ReCiPe 2016)
Solar collector		32.5 Pt/m^2
DHWT		173.1 Pt/m^3
Auxiliary boiler		$1.57 \cdot 10^3$ Pt/kW
Heat exchanger		2.515 Pt/m^2
Pump		62.8 Pt/kW
SST insulation	*XPS*	0.773 Pt/kg
	MW	0.0016 Pt/kg
	FG	0.266 Pt/kg
SST construction	*NC*	0.008 Pt/kg
	HPC	0.002 Pt/kg
	UHPC	0.0206 Pt/kg
Natural gas		0.0245 Pt/kWh
Electricity		0.0380 Pt/kWh

5.1. Robust ANN results

5.1.1. Model setting

This is the first step (step A) of the two-step approach defined in Table 1, which concerns to build a robust ANN model with an appropriate computational cost. In this stage, we evaluate the accuracy of the ANN model under three sample sizes (64, 256, 1024) using Bayesian optimization to produce an accurate metamodel independently on the model setting that can be extended to the large training set.

The solution of the Bayesian optimization is given by an interactive parallel coordinate plot to identify the suitable hyperparameters settings for the reduced number of configurations in step B (see Fig. 4). The top plot shows the total optimal Bayesian optimization results comprising 500 ANN model settings where each line represents one of these optimal solutions along with the achieved $C.V$ values. On the contrary, the bottom plot shows only the top 20% ranked optimal solutions based on $C.V$ criteria. The table below the interactive parallel coordinate plots shows the optimal metamodel setting that achieves the highest accuracy at step (A) training sets. In case of no agreement for selecting a certain optimal setting at different sample sizes, the histogram attached to each interactive parallel coordinate column is utilized to propose the most frequently setting at each hyperparameter. The hyperparameters, including the training function, number of layers, layer function, hidden function, and Momentum mean at each training set, have the same optimal setting at different training sets, whereas the number of neurons and learning rate change at each training set. As observed from the histogram, most of the optimal results setting for the learning rate are set in a range below 0.01. Thus, the learning rate is set to 0.001 for the convergence stage (step B) to sustain the training set converge. On the other hand, the number of neurons with the size of 3, 14, and 20 are set for the convergence stage (Step B) since its histogram is almost equally large for the training set size 64, 256, and 1024. A summary of the selected settings in the convergence stage (step B) is shown in the below table in Fig. 4, where the nominated settings are highlighted.

5.1.2. Sensitivity analysis

The next step is to perform the sensitivity analysis in order to investigate the relative importance of neurons sizes in step A and to eliminate the least influential variables from the convergence step (step

Table 6
Summary of uncertain parameters in the SHDS model and their characterization approaches (The parameter μ (mean) for a normal distribution (N) and (U) refers to the discrete non-probabilistic scenario).

Uncertain parameter	Parameter description	Probability distribution	Ref.
$C_{C_{COL}}$	Investment cost of the solar collector	$N(\mu, 0.07\mu)$	[41]
$C_{C_{SST}}$	Investment cost of the SST	$N(\mu, 0.07\mu)$	[41]
$C_{C_{DHWT}}$	Investment cost of the DHWT	$N(\mu, 0.07\mu)$	[41]
$C_{C_{H.E}}$	Investment cost of the heat exchanger	$N(\mu, 0.07\mu)$	[41]
C_{C_P}	Investment cost of the pumps	$N(\mu, 0.07\mu)$	[41]
C_{C_f}	Investment cost of the gas boiler	$N(\mu, 0.07\mu)$	[41]
i_f	Annual natural gas inflation rate	$N(\mu, 0.166\mu)$	[122]
i_e	Annual electricity inflation rate	$N(\mu, 0.166\mu)$	[122]
i	Annual inflation rate	$N(\mu, 0.166\mu)$	[122]
d	Discount rate	$N(\mu, 0.137\mu)$	[124]
FBM	Maintenance factor	D[1%, 1.5%, 2%]	[125]
c_f	Natural gas cost rate	$N(\mu, 0.166\mu)$	[124]
c_e	Electricity cost rate	$N(\mu, 0.166\mu)$	[124]

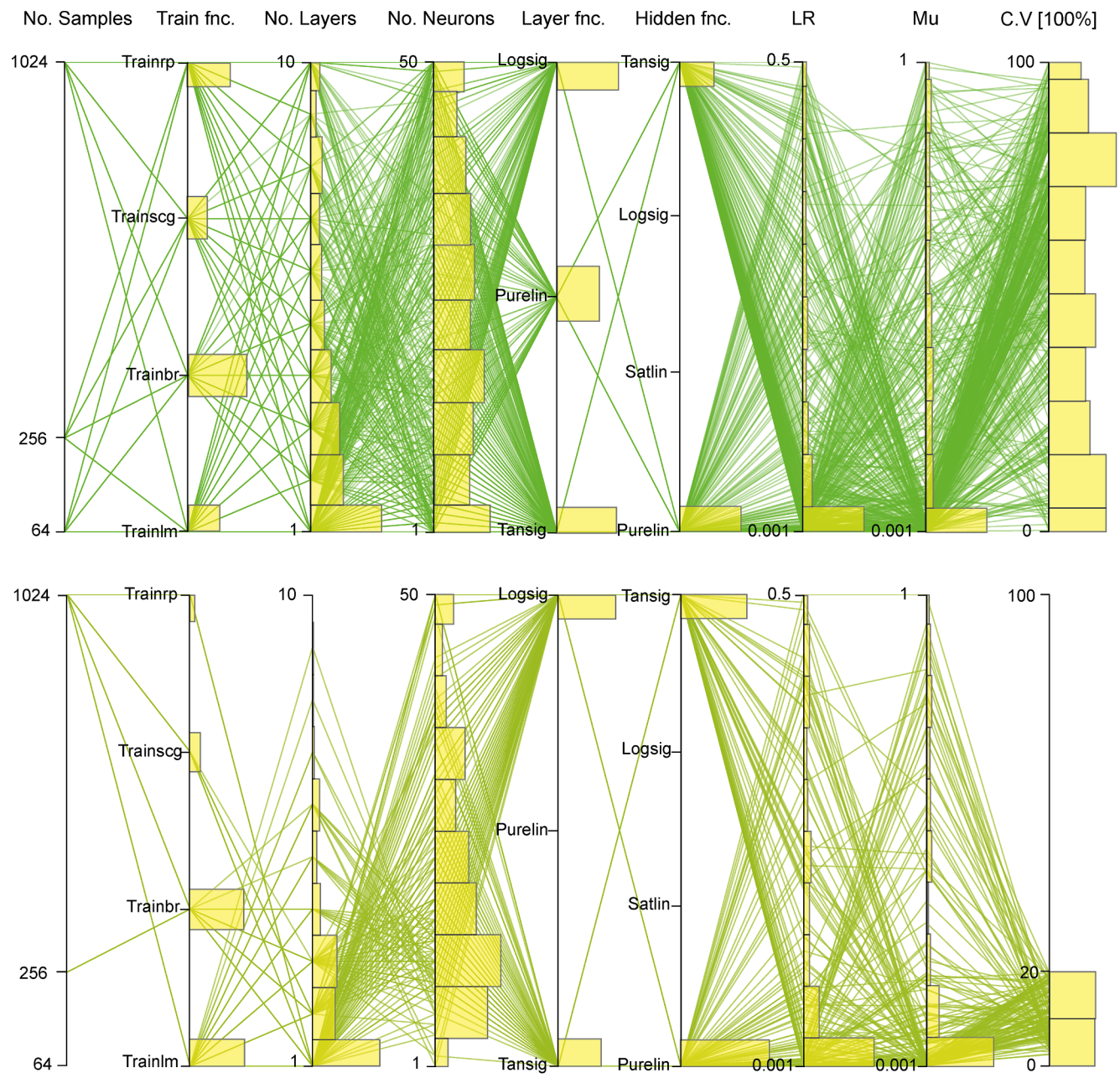

Optimal Hyperpar.	64	Trainbr	3	3	Logsig	Purelin	0.042	0.004	49.7%
	256	Trainbr	3	14	Logsig	Purelin	0.004	0.836	9.42%
	1024	Trainbr	3	20	Tansig	Purelin	0.001	0.004	2.49%

Fig. 4. Interactive parallel coordinate plots combined with histograms are utilized to identify the optimal hypermeters setting for the ANN model in step A. The top plot illustrates the total Bayesian optimal solutions without filtration, whereas the bottom plot shows the top 20% ranked ANN model settings. The table below shows the optimal hyperparameters that bounces the lowest $C.\ V$ value under different sample size where the selected setting for the convergence phase is highlighted.

B), which include more training sets to develop an independent ANN model on the sample size. In the definitive screening design, we use three training sets with a size of 64, 256, and 1024 to rank the influence of hypermeters based on the $C.\ V$ criteria. The relative sensitivity of the ANN hyperparameters is shown in Fig. 5. The training set size, training function, and momentum mean are the most significant tuning parameter with a relative sensitivity of 28%, 26%, and 24%, respectively. These high impact parameters are followed by the number of neurons, which has a relative impact of 10% on the $C.\ V$. Thus, varying number of neurons may contribute to enhance in the performance of ANN model in step B. On the other hand, the activation functions, and the learning rate seems to be insignificant since they have only a contribution of 3% and 2%, respectively to the $C.\ V$ value. The results confirm the possibility of fixing the learning rate without affecting the surrogate model accuracy.

Following the sensitivity analysis results, a box plot (Fig. 6) is built to show the performance of the three-training sets (64, 256, and 1024) based on the $C.\ V$ rank under the optimal selected hyperparameters with considering for three neurons sizes comprising 3, 14, and 20 in comparison to the default settings. The box plot is characterized by the central mark, the upper and lower quartiles which correspond to the box edge. While the minimum and maximum optimal values are

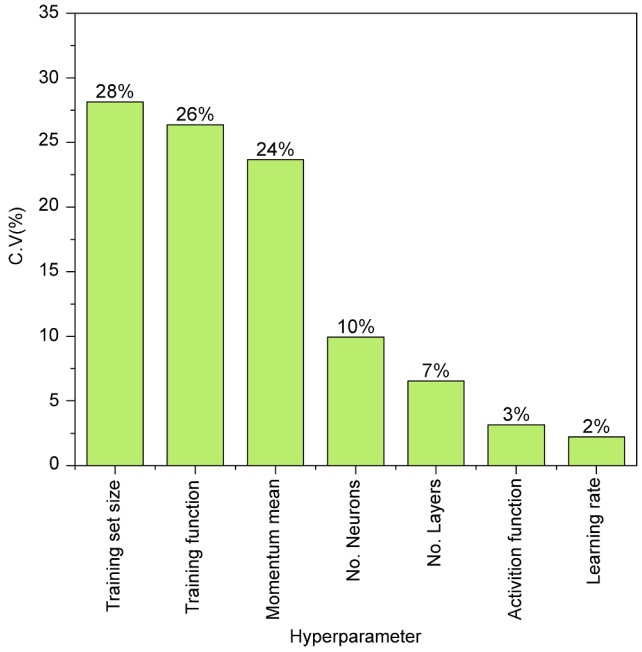

Fig. 5. The definitive screening design for the ANN hyperparameters.

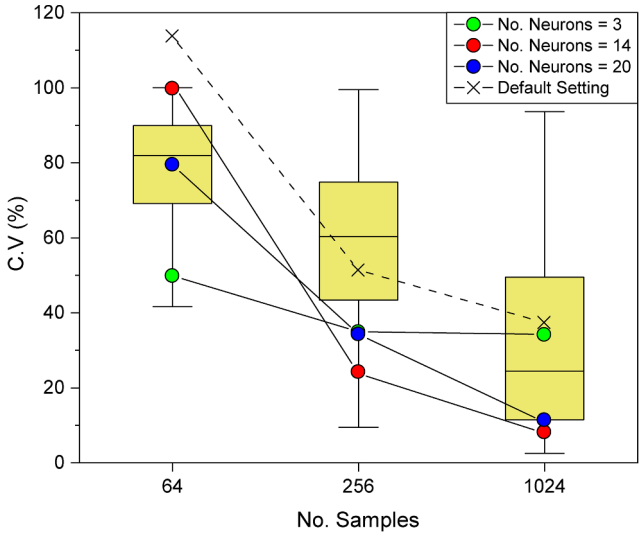

Fig. 6. Box plot for the output in step A including the ANN model performance under the optimal and default settings.

indicated at the whiskers. On the plot, the lined circles at each sample size show the results under optimal settings at a different number of neurons, whereas the cross symbols represent the results at the default settings. In general, the default setting does not yield to build accurate ANN models that approve the importance of tuning the hyperparameters. Moreover, fixing the number of neurons at 14 provides the most accurate results with a *C. V* value of 24.1% and 9.2% for the 256 and 1024 training set, respectively.

5.1.3. Convergence with a variable training set

In step B, we test the performance of the selected optimal hyperparameters at various training sizes in order to choose the most accurate ANN model with consideration for its efficiency in terms of the computational cost, as shown in Fig. 7. In terms of convergence, as mentioned in the methodology section, three accuracy criteria comprising the $R^2 - adj.$, *C. V* and *SMAPE* are utilized to evaluate the performance of the ANN model. The results show that the $R^2 - adj.$ is a

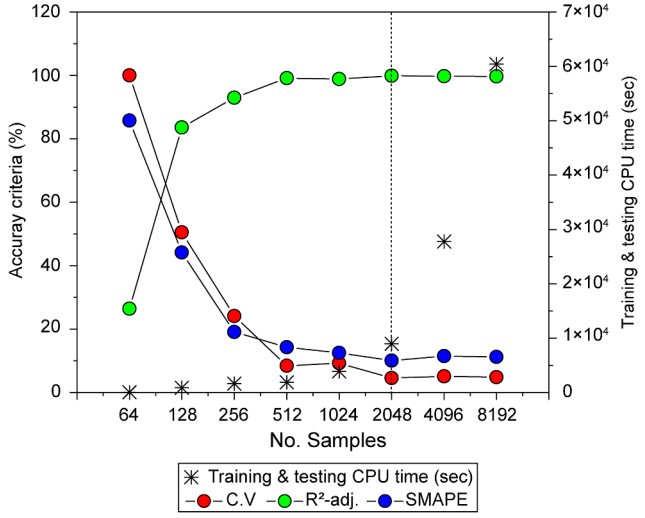

Fig. 7. Convergence of accuracy criteria at various training size with consideration for its relative computational cost.

misleading criterion since most of the sample sizes excess 97%. Therefore, using *C. V* and *SMAPE* can be more efficient to measure the ANN model accuracy. Increasing the sample size has a clear tendency to improve the ANN model accuracy where the highest accurate value of 4.5% and 10% was indicated in a sample size of 2048 for the *C. V* and *SMAPE* criterion, respectively. In terms of the ANN model computational cost, an exponential behavior is indicated with increasing the sample size where the CPU time at 8192 sample size is 6×10^4 sec. Comprising the model accuracy with its efficiency simultaneously, the sample size 2048 provides the highest accuracy at an affordable computational time of 8.9×10^3 sec using an Intel® Xeon® E5-2620 v4 2.10 GHz processor with 32.0 GB RAM.

A breakdown for the ANN model performance in comparison to the rigorous model based on TRNSYS at a sample of the outputs is shown in Fig. 8. In general, an agreement between the rigorous and ANN model results is indicated for the 19 output where the $R^2 - adj.$ is almost 99% for the whole outputs. To gain further confidence in the ANN model performance, the model accuracy is also presented through the *C. V*, which doesn't get below 5.3% for the model outputs.

The proposed robust surrogate model built based on the two-model steps comprising the sensitivity analysis offers a sufficient approach for the construction of fast metamodels to overcome the computational barrier related to design space exploration, design optimization, and sensitivity analysis of heuristics optimization models.

5.2. Optimization results

Once a robust ANN model is built independently on its tuning parameters (Hyperparameter) with the consideration for the model accuracy simultaneously with its efficiency, the ANN model is coupled with a MOGA in order to investigate the capability of the develop simulation-optimization framework in tackling the technical performance of the SDHS in cooperate with its economic and environmental impact at various community sizes. The optimization problem has two main stages; the first stage is devoted to analyze the effect of expanding the decision variables through including the seasonal TES geometry and its construction design parameters in the optimization problem. While the second stage is dedicated to examine the community size effect in the performance of the SDHS. In general, the optimization results are presented in five scenarios; these scenarios are:

- Scenario 1: No environmental damage limits (Min. cost).
- Scenario 2 to 4: 25%, 50%, and 75% damage reduction against the 1st scenario, respectively.

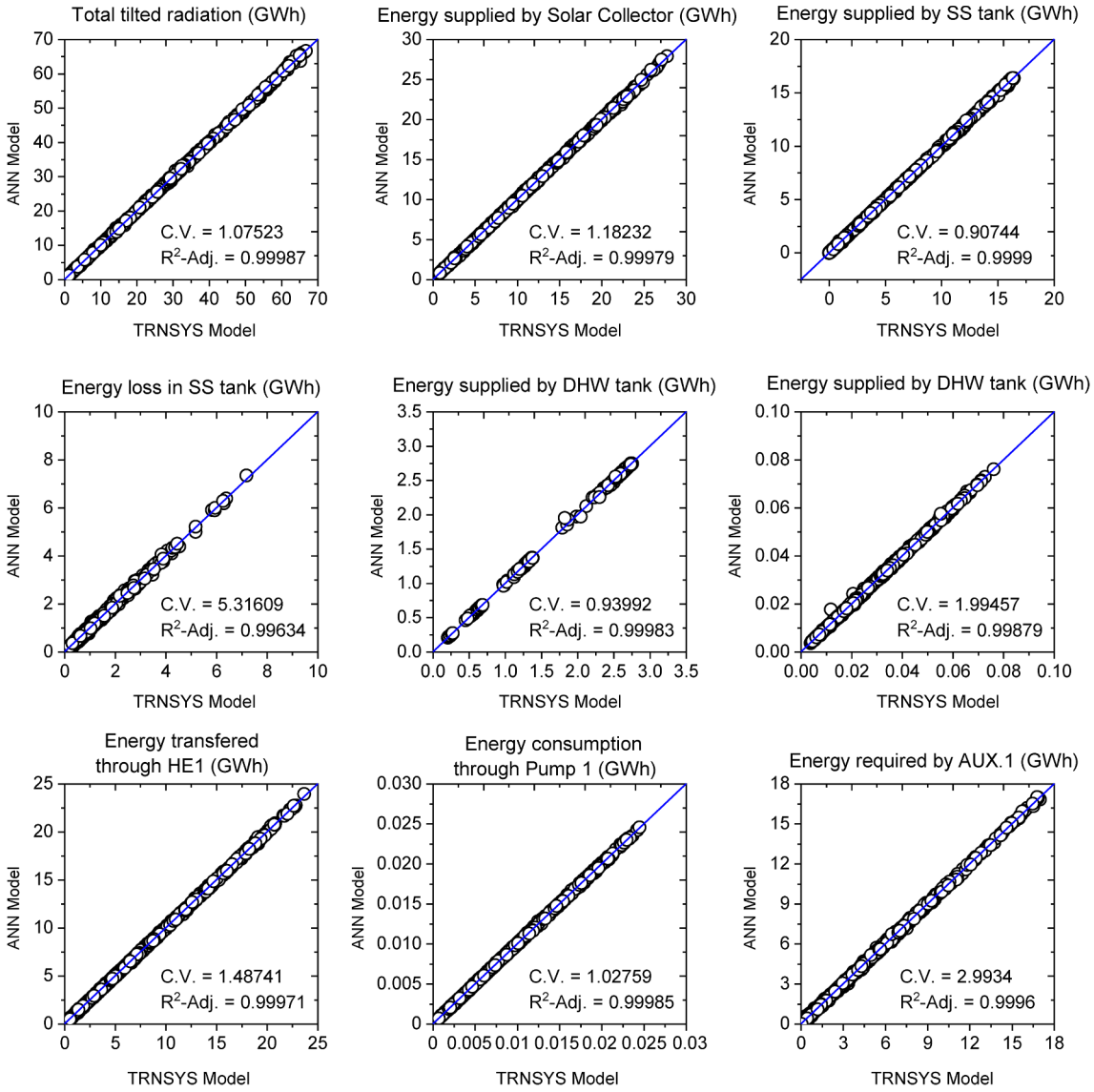

Fig. 8. Parity plots showing the performance sample of ANN model versus the TRNSYS model for the SDHS.

- Scenario 5: 100% of the environmental damage limits (Min. impact).

5.2.1. Influence of the SST design parameters (geometry & construction)

In this stage, the capability of the developed framework is tested through Madrid case study at a small community size of 10 buildings. The optimization problem is formulated under two main settings:

- Partial decision variables (PDV) – 8 decision variables: In this setting, only the equipment sizes are considered as decision variables in the optimization problem without consideration for the insulation material configuration and construction material of the SST. Thus, the construction of the SST is fixed based on the Friedrichshafen project [22], in which the NC has been used as the main construction material. While, the MW with a thickness of 0.3 m, 0.2 m, and 0.2 m is utilized for the roof, wall, and ground, respectively.
- Full decision variables (FDV) – 15 decision variables: In this setting, the SST design variables are considered as well in formulating the optimization problem in order to investigate the impact of SST geometry and its construction in improving the SDHS optimal solutions.

Fig. 9 shows the optimal system cost in terms of *NPC* and its environmental impact in term of *RCP* under various scenarios. While the base case corresponds to the conventional system. A clear tradeoff between the proposed objective functions is indicated since the movement from scenario 1 to 5 at both PDV, and FDV settings increase the total cost while minimizing the environmental impact. Under the PDV setting, replacing the base case (Natural gas boiler) with SDHS can extensively minimize the environmental impact by 79.4% in scenario 1 (Min. cost). Using the latter value, the environmental impact for scenarios 2 to 5 improved by 80.8%, 83.3%, 85.1%, and 87%. On the other hand, the Pareto optimal solutions at small community size (10 buildings) under PDV setting couldn't provide a marginal economic benefit since only scenario 1 minimizes the economic cost by 22% whereas the economic cost increases by 10.2%, 35.5%, 49.9% and 61.7% for scenarios 2 to 5, respectively.

Under the FDV setting, more enhancement is indicated in both objective functions in comparison to the PDV optimal Pareto solution due to including the SST design parameters in the optimization problem. In scenario 1, the *NPC* is equal to 62.5 €/MWh which is less than the PDV Min. cost solution by 11.1%, whereas the environmental impact (*RCP*) is 5.49 Pt/MWh which increases the *RCP* by 0.18% compared to the

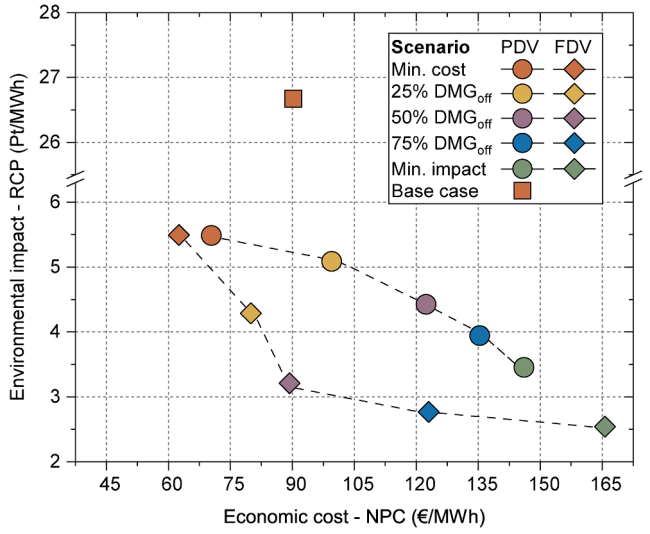

Fig. 9. Pareto sets for optimal SDHS solutions under PDV and FDV settings. These solutions cover the SH and DHW demand of 10 buildings located in Madrid at different scenarios in comparison to a conventional solution based on natural gas.

PDV setting. With increasing the environmental damage limits from scenario 2 to 4 under the FDV setting, the *NPC* decreases by 19.6%, 27%, and 9.4% whereas the Min. impact solution increase the total cost by 13.4% in comparison to the PDV setting. Furthermore, following scenario 1 under the FDV setting, the environmental impact is improved by 15.7%, 27.3%, 29.7%, and 26.4% for scenarios from 2 to 5. This improvement increases the competitivity of the SDHS compared to the conventional systems based on natural gas.

Following that, each Pareto optimal solution under PDV and FDV settings represents a specific configuration for the SDHS to cover the SH and DHW demand of a small urban community (10 buildings) located in Madrid. Fig. 10 shows the selected feature for each decision variable from scenario 1 to 5 under PDV and FDV settings. In both optimization settings, increasing the damage limitations causes an increment in the share of renewable energy equipment. Under the PDV setting, the solar collector share increases from 0.4 m^2/MWh/a at scenario 1 to 1.33 m^2/MWh/a at scenario 5.

Furthermore, the SST volume increases from 2.3 m^3/MWh/a for Min. cost solution to 11.9 m^3/MWh/a at the Min. impact solution. Including the SST design parameters in the optimization problem (FDV setting) shows a different configuration for SDHS where the solar collector share increases only from 0.54 m^2/MWh/a at scenario 1 to 1.17 m^2/MWh/a at scenario 5. While the SST volume share increases from 4.96 m^3/MWh/a at scenario 1 to 13.7 m^3/MWh/a at scenario 5 with an increment of 13.2% compared to the PDV optimization setting. Regarding the SST construction, the UHPC shows superiority over other construction materials at all scenarios under the FDV setting. Moreover, the foam glass gravel is utilized as an insulation material for all SST surfaces except the min impact solution, which uses mineral wool due to its lower environmental impact. For the insulation thickness, all Pareto optimal solutions under FDV settings increase the walls insulation thicknesses to be varying between 0.3 and 0.73 at all scenarios. Regarding the SST geometry, the HDR varies between 0.62 and 0.68 with a limited difference from the PDV settings. Moreover, the DHWT volume is almost constant for the proposed settings where its volume varies only between 0.09 and 0.13 m^3/MWh/a.

To facilitate a complete economic analysis of the SDHS, Fig. 11 shows a comprehensive breakdown for the cost contribution of each equipment in the SDHS throughout its operation lifetime under PDV and FDV optimization setting together with the base case solution. As shown in the figure, the contribution of the SDHS initial capital cost under the PDV and FDV optimization settings is very high in comparison to the base case solution. This expansion is due to the deployment of solar energy equipment in the district heating system, which requires high investment cost. To be more specific, the solar collectors, heat exchangers, and SST have the main contribution to the initial capital cost. Under the PDV optimization setting, the movement from scenario 1 to 5 (Min cost to Min. impact optimal solution) expands the usage of solar collectors and SST due to its advantage in diminishing the contribution of using the auxiliary heater based on natural gas. In scenario 1, the solar collector and SST have contributions of 5.30% and 29.2%, respectively. These contributions are expanded to 6.94% and 39.7% in scenario 5. On the other hand, under the FDV optimization setting, with

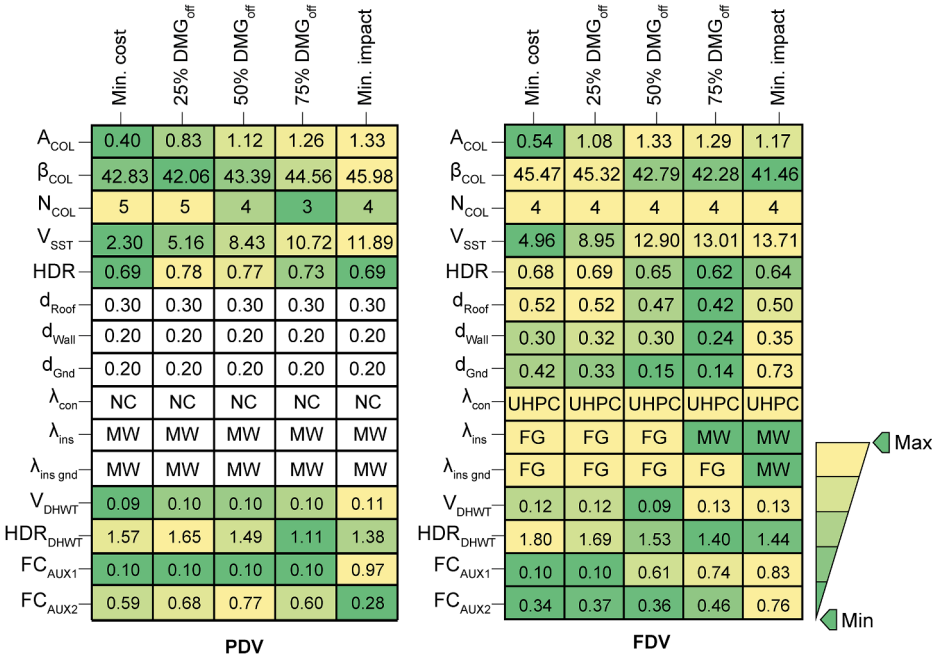

Fig. 10. Pareto optimal solutions of SDHS configuration to cover the demand of 10 buildings located in Madrid under PDV and FDV setting where the color map indicates the min and max value of each decision variable and the white boxes indicated the fixed parameters in the PDV optimization setting.

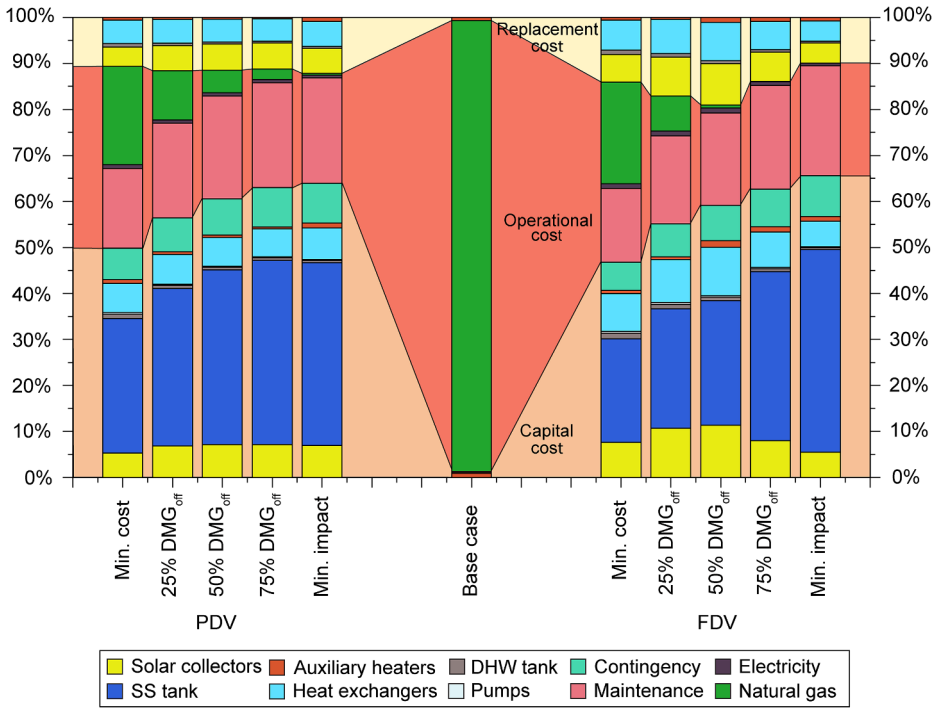

Fig. 11. Breakdown of the *NPC* including the shares of initial capital cost, operational cost, and replacement cost for Pareto optimal solutions under the PDV and FDV optimization settings at the 5 optimal scenarios in comparison to its relative base case. These solutions cover the SH and DHW demands of 10 residential building located in Madrid.

the opportunity to include the construction materials of the SST in the optimization framework, the initial investment cost can be relatively reduced compared to the PDV optimization Pareto solution where the SST contribution is only 22.5% in the scenario 1 (Min. cost), and it expands to 44% in the scenario 5 (Min. impact). Furthermore, the solar collector has relatively more contribution under the FDV optimization setting, where the solar collector contribution expands from 7.60% in scenario 1 to 8.04% in scenario 4. However, this expansion bounds to only 5.50% in scenario 5 (Min. impact). In the replacement cost, the same behavior is noticed under the PDV and FDV optimization setting, where a significant contribution is observed due to the solar energy equipment in comparison to the base case solution. On the contrary, the operational cost has a predominant contribution of 98.2% in the base case solution due to usage of natural gas, these contribution shrinkages

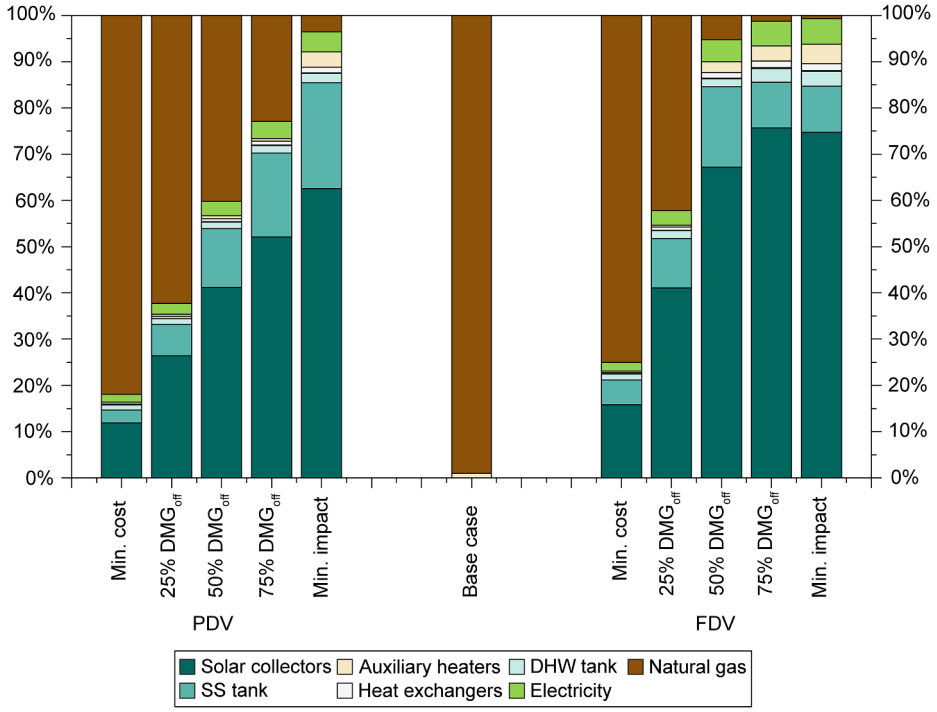

Fig. 12. A breakdown for the aggregated ReCiPe 2016 environmental impact of the optimal Pareto solutions under PDV and FDV optimization settings in comparison to their respective base case. These solutions comprise configurations to satisfy the SH and DHW demand of 10 residential building located in Madrid.

under the PDV and FDV optimization setting where the operational cost in scenario 1 represents around 39% in both optimization settings. With the increment in the environmental damage limits (scenario 2 to 5), less contribution to the operational expenses is noticed for both optimization settings where the operational cost in scenario 5 represents only 24% due to the reduction in using Natural gas. The reduction will be reflected in the environmental impact of the SDHS optimal solutions.

In addition to the economic analysis, Fig. 12 offers a detailed analysis for each equipment in the SDHS based on the aggregated ReCiPe 2016 in comparison to the base case using natural gas. In this figure, the natural gas consumption in the base case represents almost 100% of the total impact. Under the PDV optimization setting, the SDHS optimal Pareto solutions are able to reduce the environmental impact up to 87.1%. This reduction value can increase up to 90.4% under the FDV setting. In scenario 1, the system relies heavily on natural gas, which corresponds to 81.9% and 74.9% of the environmental impact under the PDV and FDV optimization setting, respectively. From scenario 2 to 5, the natural gas impact diminutions progressively with the increment in the environmental limits. Along with the reduction in the natural gas impact share, a progressive rise is indicated in the renewable energy impact where the solar collectors and SST share the most contribution to the aggregated environmental impact especially with introducing the SST construction materials in the optimization problem (FDV optimization setting).

As shown in Fig. 13, the thermal performance of the proposed SDHS is evaluated through a combination of nominal performance indicators; these indicators comprise the main renewable energy equipment efficiencies and their relative solar fractions. Under both optimization settings, a limited change in the η_{COL} is indicated with the change in scenarios, where the highest η_{COL} is indicated in the scenario 1 due to the limited utilization of solar collector. Moreover, the DHWT is utilized for daily purposes without storage; thus, a limited heat loss to the environment is indicated in all scenarios. This can be reflected in the DHWT efficiency, where η_{DHWT} is around 96% for all scenarios under both optimization settings. Regarding the SST performance, under the PDV optimization setting, with almost a constant value for the heat loss coefficient of around 0.16 W/m^2·K for all scenarios, the annual SST heat losses remain above 33 kWh/m^3 with a narrow variation with the increment in the environmental limits. Also, the η_{SST} remains around 71% for all scenarios except scenario 1 where the η_{SST} is 67%. In terms of the solar fraction, the contribution of the DHW distribution circuit remains above 98% for all scenarios, whereas the *S*. F_{SST} rises progressively with the increment in the environmental damage limits (increment in the usage of renewable energy equipment) where solar fraction increases from 80% in scenario 1 (Min. cost) to 99% in scenario 5 (Min. impact).

Under the FDV optimization settings, with the change in the SST construction materials and its geometry, the heat loss coefficient of the SST reduces from 0.15 in scenario 1 to 0.08 W/m^2·K in scenario 5. This reduction is reflected in the SST heat losses, which diminish gradually with increasing the environmental damage limits, and it reaches 18 kWh/m^3 with an improvement of 45.2% compared to the same scenario under the PDV optimization setting. This improvement is emulated in the η_{SST} especially in the two extremes optimal scenarios (Min. cost and Min impact optimal solutions) where the η_{SST} improved by 4.5% and 12.3% in scenario 1 and 5, respectively. In terms of the solar fraction for both SH and DHW distribution circuits, the same progressive behavior is indicated under the FDV optimization setting with a slight improvement of 2.5% in scenario 1 in comparison to the PDV optimization setting.

5.2.2. *Influence of the community size*

Following the performance analysis for the SDHS under PDV and FDV optimization settings in the small urban community with 10 buildings, the proposed framework based on a MOO approach is expanded to be applied for different urban community sizes. This approach examines the community size effect (10, 25, 50, and 100 buildings) on the performance of the SDHS in a techno-economic optimization framework with consideration for its environmental impact.

Fig. 14 shows a clear tendency between the objective functions and the increment in the community size, where increasing the community size raises the economic and environmental benefits in comparison to their relative base cases. Following the small urban community size (10 building), under the PDV optimization setting, the *NPC* in the Min. cost solutions is improved by 26.8%, 34.7% and 53.9% for the 25, 50 and

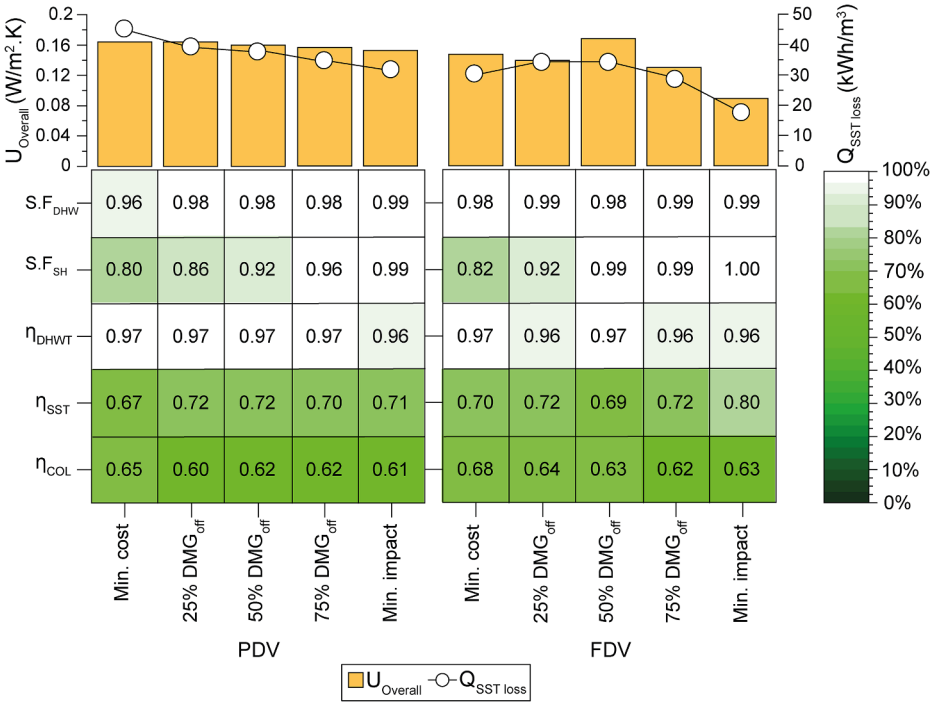

Fig. 13. Thermal performance indicators for the optimal Pareto SDHS solutions under PDV and FDV optimization settings. These designs satisfy the SH and DHW demand of the 10 residential buildings located in Madrid.

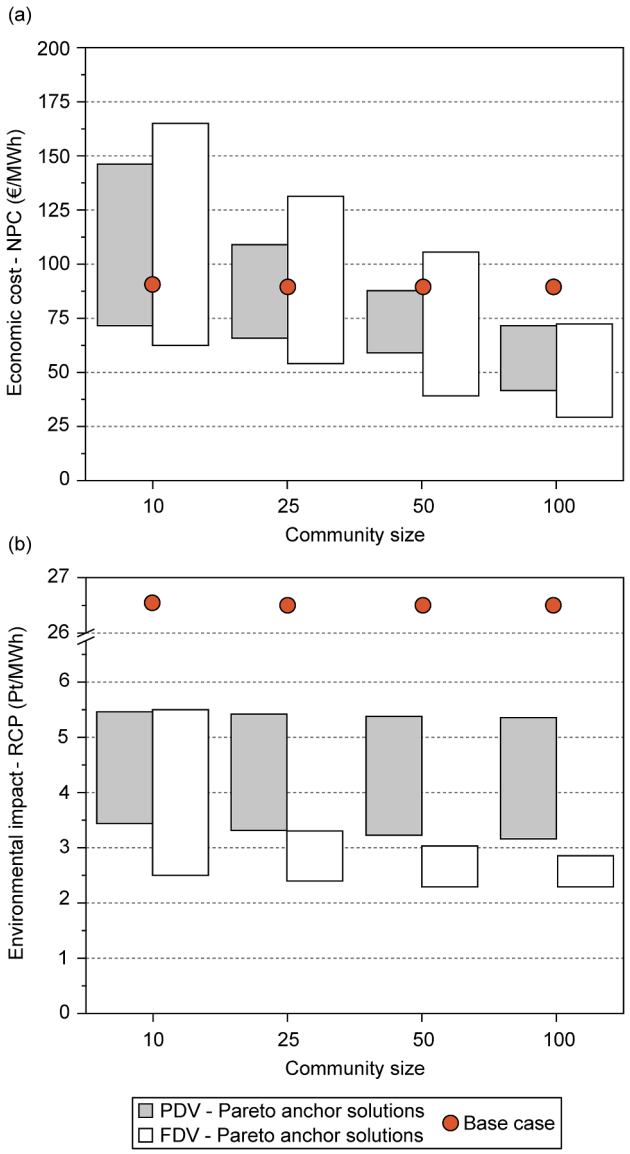

Fig. 14. Various Pareto optimal solutions for the SDHS in different community sizes covering the SH and DHW yearly demand in comparison to their respective base case using natural gas, (a) Economic optimal solution of SDHS at the different scenarios under PDV and FDV optimization setting, (b) Environmental optimal solution of SDHS at the different scenarios under PDV and FDV optimization setting.

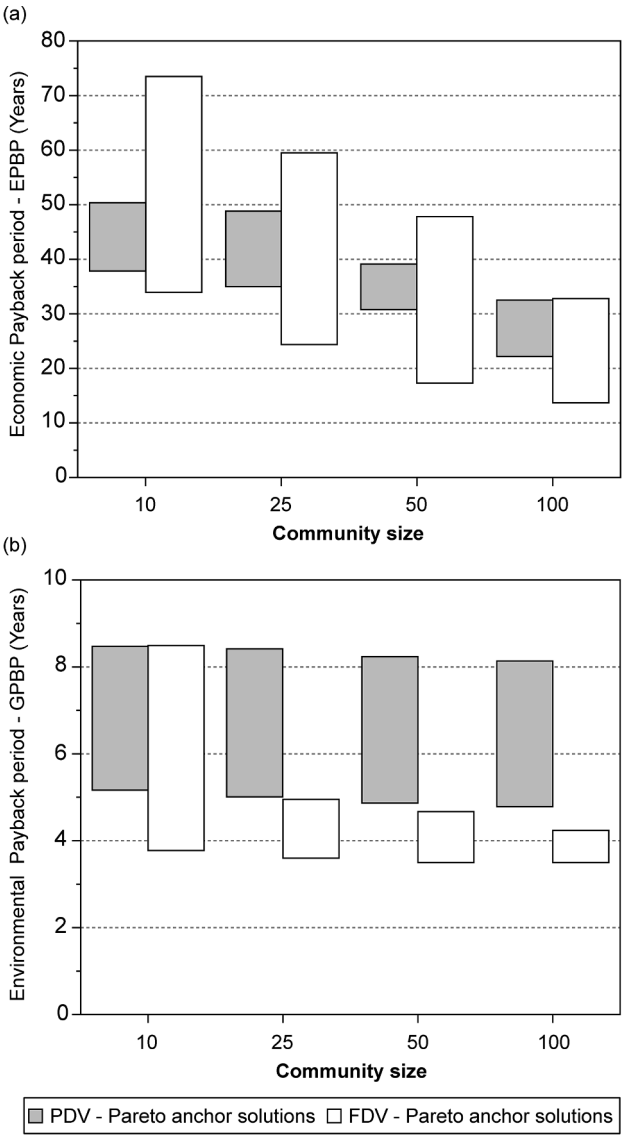

Fig. 15. Various Pareto optimal solutions for the SDHS in different community sizes covering the SH and DHW yearly demand in comparison to their respective base case using natural gas, (a) Economic payback period of the SDHS at the different scenarios under PDV and FDV optimization setting, (b) Environmental payback period of the SDHS at the different scenarios under PDV and FDV optimization setting.

100 buildings, respectively in comparison to their relative base cases. On the other hand, the economic competitivity of the Min. impact solution is restricted where at the 25-building community, the *NPC* increases by 21.3% in comparison to its base case. With increasing the community size above 25, the *NPC* of the Min. impact solution decreases by 2.3%, and 19.7% for 50 and 100 community size, respectively. Under the FDV optimization setting, a slight improvement is indicated in the *NPC* of the Min. cost optimal solution with increasing the community size where it improved by 18.1%, 35.9%, and 26.8% for building community size of 25, 50, and 100, respectively compared to the optimal solutions under PDV optimization setting. Furthermore, adding the construction materials of the SST in the optimization problem demonstrate a limited improvement in increasing the competitivity of SDHS against the natural gas solution where the Min. impact solution only improved by 1.85% at community size of 100 buildings compared to the same optimal solution under PDV optimization setting.

The optimal environmental impact of the SDHS in different community sizes follows the optimal solutions of the 10 buildings located in Madrid, where the SDHS is beneficially effective in reducing the environmental impact compared to the conventional system using natural gas. Under the PDV optimization setting, the optimal Min. cost solution reduces the environmental impact by 79.5%, 79.6%, and 79.7% for the urban community size of 25, 50, and 100 buildings, respectively. Besides, the optimal Min. impact solution extensively reduces the environmental damage by 87.4%, 87.7, and 88% for the 25, 50, and 100 buildings, respectively. These results approve a limited improvement in the environmental impact of the optimal SDSH solutions with the increment in the community size under the PDV optimization setting. Under the FDV optimization setting, the environmental benefits of replacing the conventional system based on natural gas with SDHS can progressively rise with increasing the community size compared to the optimization problem under the PDV setting. The optimal Min. cost solutions are improved by 87.4%, 88.4%, and 89.3% for an urban community of 25, 50, and 100 buildings, respectively. This improvement is expanded as well for the Min. impact solution where an

improvement around 43.3% is indicated for all community sizes compared to the Min. impact optimal solutions under the PDV optimization setting.

In addition to evaluating the economic and environmental performance of the SDHS based on the *NPC* and *RPC* indicators, respectively, the *EPBP* and *GPBP* are proposed to measure the system sustainability throughout its lifetime from the economic and environmental perspective under the PDV and FDV optimization settings at in different community sizes as shown in Fig. 15. In terms of the economic payback period, the SDHS could not approve its feasibility in the community size of 10 buildings, especially under the PDV optimization setting where the *EPBP* is varying between 38 years and 51 years, which is higher than the lifetime of the SDHS. Under the FDV optimization setting, the SDHS feasibility increased, especially in the low environmental damage scenarios where the*EPBP* in Min. cost optimal solution is 33 years. With increasing the community size, the *EPBP* decreases progressively. Under the PDV optimization setting, the *EPBP* at the Min. cost optimal solution reduces to 35, 31, and 22 years for the community size of 25, 50, and 100 buildings, respectively. While under the FDV optimization setting, more improvement in the *EPBP* can be indicated where the *EPBP* in the Min. impact optimal solution reduces to 25, 17, and 14 years for the community size of 25, 50, and 100 buildings, respectively. In terms of the *GPBP*, a limited improvement can be indicated with increasing the community size under the PDV optimization setting due to the absence of the SST construction materials in the optimization framework. In the Min. impact optimal solution, the *GPBP* is around 5 years for all community sizes. While under the FDV optimization setting, the *GPBP* reduces to only around 3 years for all community sizes. Moreover, an extensive improvement in the Min. cost solutions at the community size of 50 and 100 buildings are shown compared to its relative optimal solutions under the PDV optimization setting where the *GPBP* reduces by 43.1% and 47.7% for the 50 and 100 buildings, respectively.

Following the advantage of including the SST construction materials in the optimization problem to improve the objective functions' performance, the proposed methodology offers a complete depiction of the features and configurations of the optimal Pareto solutions categorized by the circuit at different scenarios under the FDV optimization setting as shown Fig. 16. This figure tends to show the most frequent selected decision variables at different community sizes under various damage scenarios. This is implemented through combining the Interactive parallel coordinate, which shows the nominated decision variables under different damage scenarios with a histogram at each Interactive parallel coordinate column to show the most common size for each decision variable. In the solar circuit, most of the optimal Pareto solutions at different community sizes remain the A_{COL} at a narrow range

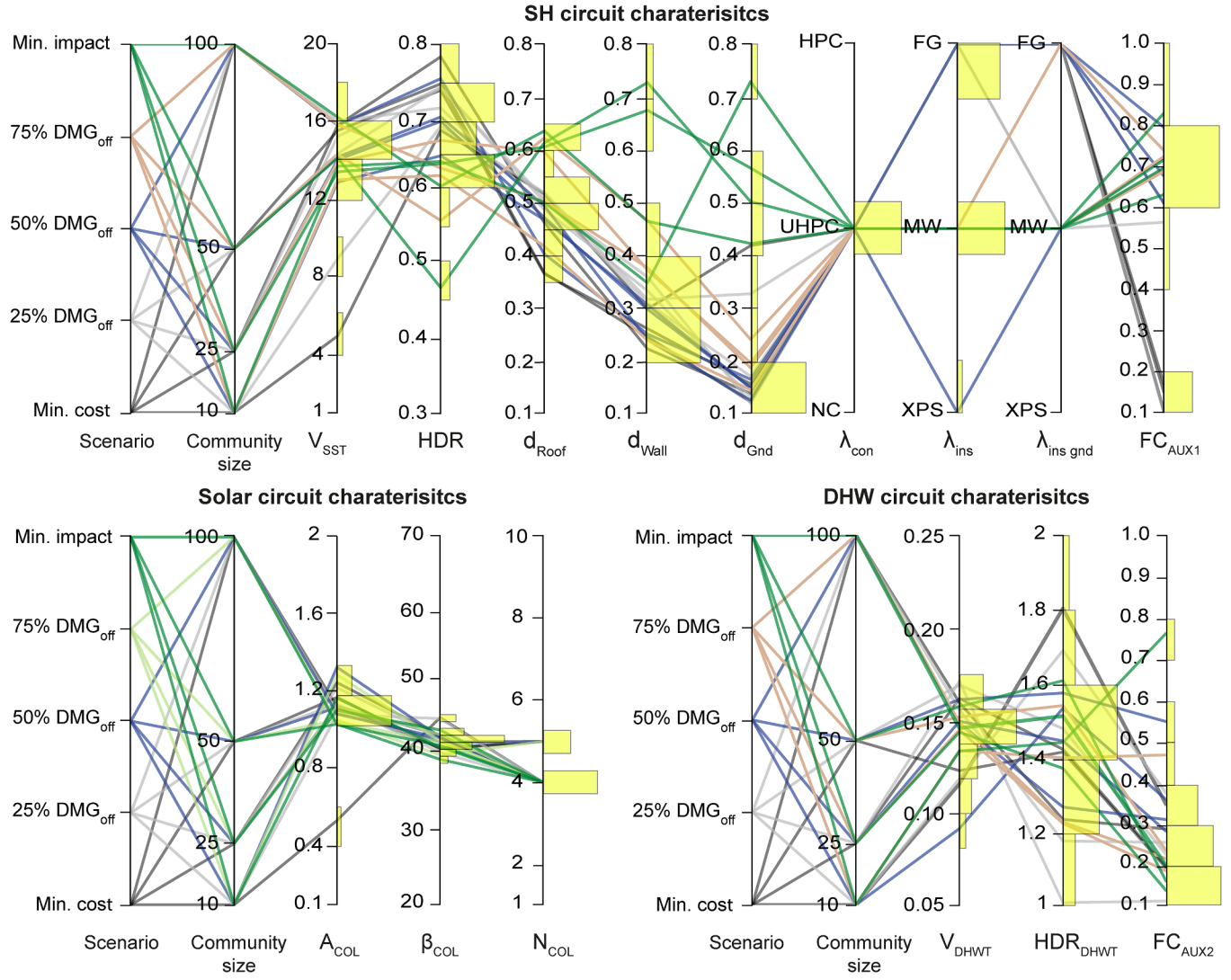

Fig. 16. Interactive parallel coordinate plots combined with histograms (Yellow bars) to identify the optimal range for the decision variables of the SHDS categorized by circuit name at different scenarios and different urban community sizes under the FDV optimization setting.

of 1.1 ± 0.1 m^2/MWh/a. Following the previous recommendation by Tulus et al. [38], the optimal inclination angles of the solar collectors (β_{COL}) stayed at an angle of 43° for most of the community sizes, which is close to the latitude of Madrid. Moreover, the number of solar collectors connected in series remains at 4 for most of the scenarios. In the DHW circuit, since the DHWT is used only for the daily purposes without long term storage, the histogram depicts that the V_{DHWT} is only around 0.15 m^3/MWh/a for most of the optimal solutions, whereas the

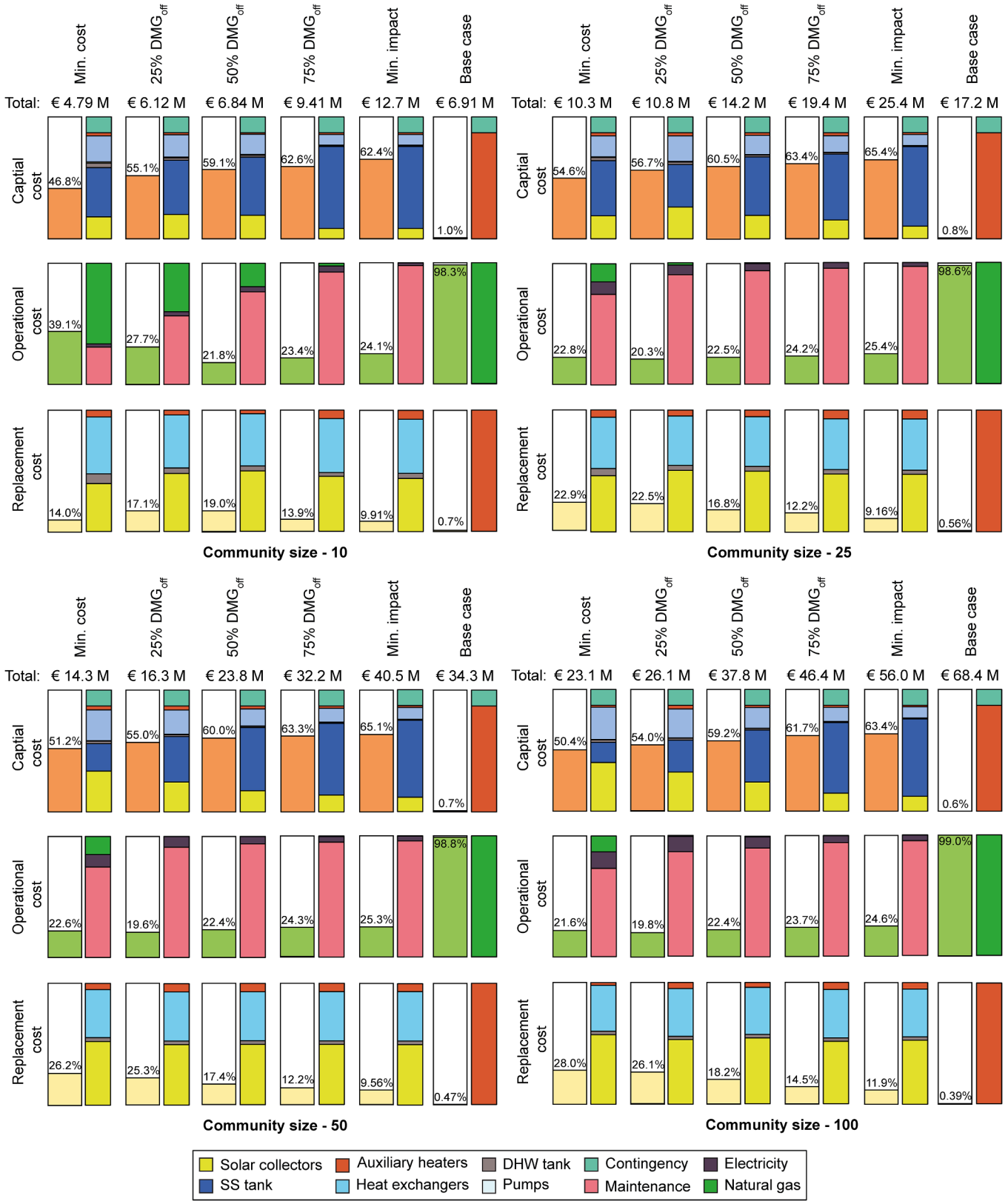

Fig. 17. Life cycle cost breakdown of Pareto optimal solutions at different scenarios for a SDHS system applied at various community sizes. The breakdown includes the shares of initial capital cost, operational cost, and replacement cost under the FDV optimization setting in comparison to their relative base case.

HDR_{DHWT} diverge around 1.5 ± 0.1 m/m. In the SH circuit, the optimal characteristics of the SST geometry at various community sizes shows that the V_{SST} is around 15 ± 1 m^3/MWh/a, whereas the HDR is around 0.65 ± 0.1 m/m for all environmental damage scenarios.

In terms of the SST construction materials, the UHPC shows superior performance in all optimal solutions due to its techno-economic advantage combined with its limited environmental impact. For the insulation materials, no agreement can be indicated for all optimization scenarios. In scenarios 1 and 2 (low environmental damage limits), the foam glass gravel with thermal conductivity of 0.06 W/m·K is chosen as insulation material for all surfaces of the SST at each community size. While moving toward higher environmental limit scenarios, most of the optimal solutions insulate the SST surfaces using mineral wool with a thermal conductivity of 0.04 W/m·K, due to its limited environmental impact. Furthermore, the insulation thickness is around 0.5 ± 0.05 m for the top roof of SST based on the scenario and the community size. This range changes to 0.3 ± 0.1 m for the SST wall, whereas it remains around 0.15 ± 0.05 m for the SST ground. Regarding the capacity of the auxiliary heater, the FC_{AUX1} is varying around 0.7 ± 0.1. These configurations of the SDHS circuit will be reflected in the *NPC* and *RCP* breakdown at different community sizes.

Fig. 17 shows a comprehensive economic breakdown for each component in the SDHS during its lifetime based on the *NPC* when applied at different community sizes under the FDV optimization setting. Similar to the small community size (10 buildings), the initial investment cost and the replacement at all other community sizes is a quite large cost component compared to their relative base cases. This cost contribution is ascending increases with raising the environmental damage limits. To be more specific, the solar collector and SST have the main contribution to the initial investment cost. Following the 10 buildings case, the community size of 25 buildings shows a significant contribution to the SST in all scenarios. This contribution declines with increasing the community size, especially in the Min. cost Pareto optimal solutions, where the SST represents only 21.9% and 16.3% of the initial investment cost for the community size of 50 and 100 buildings, respectively. This drop is due to the possibility of changing the SST construction, which can contribute to reduce the initial investment cost of the SST. For the operational cost, the Min. cost-optimal solution at a

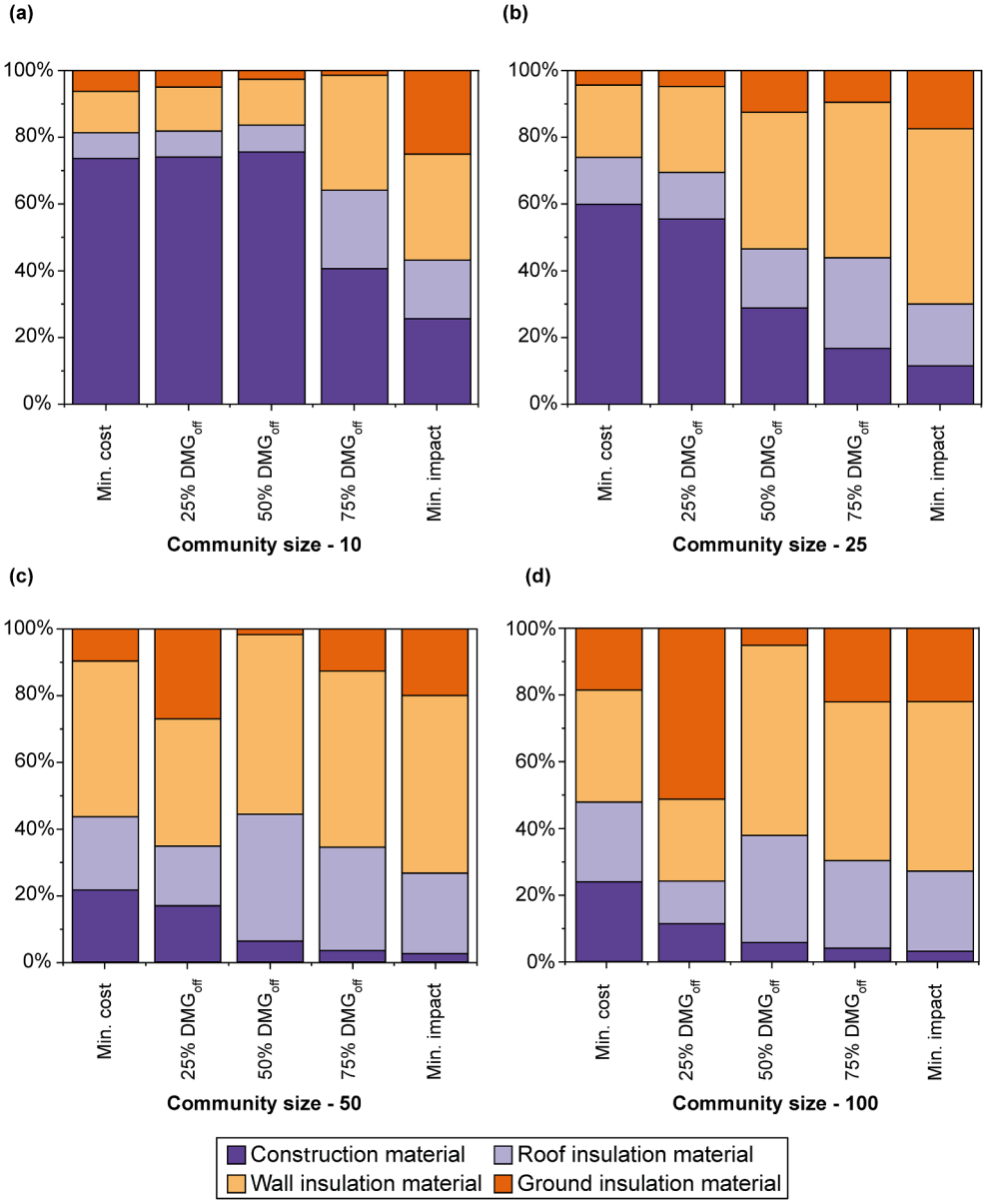

Fig. 18. Life cycle cost breakdown for the SST at different community sizes under different damage scenarios for (a) 10 buildings, (b) 25 buildings, (c) 50 buildings, and (d) 100 buildings.

community size of 25 buildings represents 22.8% of the total cost. This is due to the dependency of the system on using renewable energy components, where the natural gas represents 12.7% of the total operational cost. With the increment in the community size, the dependency on using natural gas becomes less compared to the small community size (10 buildings) due to the feasibility of introducing the

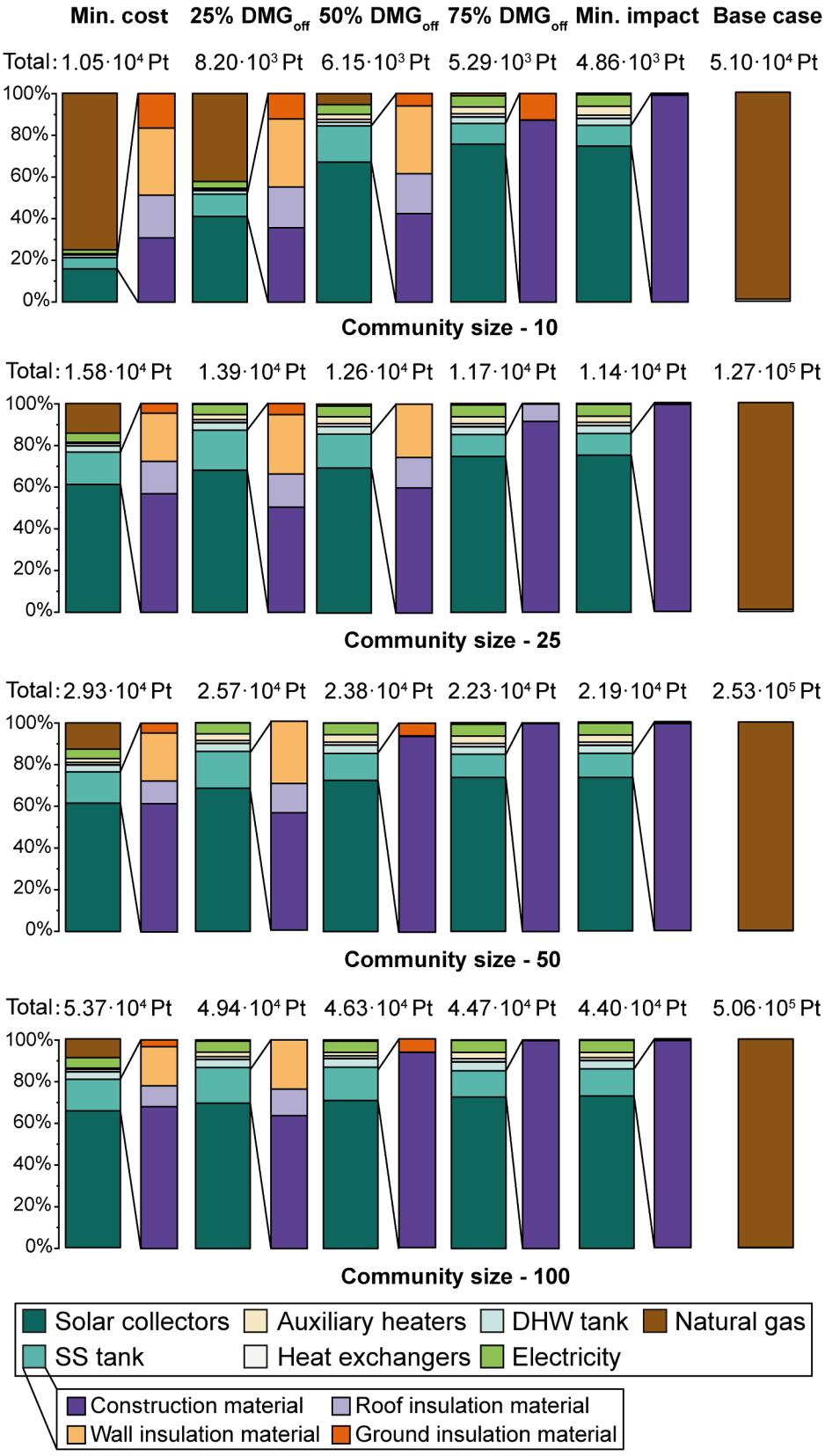

Fig. 19. A breakdown for the aggregated ReCiPe 2016 of Pareto optimal solutions at different scenarios for the SDHS system applied at various community sizes. The breakdown includes the share of the SST construction components under the FDV optimization setting in comparison to their relative base case.

renewable energy components even in the Min. cost-optimal solutions. Thus, the operational cost due to natural gas represents only 16.9% and 13.8% for community size of 50 and 100 buildings, respectively.

Following the effect of introducing the SST construction materials in improving the performance of the objective functions, Fig. 18 depicts a detailed breakdown for the SST life cycle cost when introduced at different community sizes. For a community size of 10 buildings, all scenarios except the scenario 4 and 5 show almost the same contribution for the SST breakdown cost where the construction materials represent around 70%. While this value drops to only 40.6% and 25.6% in scenarios 4 and 5, respectively, and the remain contribution is dedicated to the insulation materials, especially the wall insulation materials, which represent around 33% of the total SST cost for both scenarios. In all other community sizes, the construction materials contribution is descending drops with the increment in the environmental damage limits and community size where it reduces from 59.8% to 11.4% at the community size of 25 buildings, and it drops to only 2.48% and 0.08% in Min. impact optimal solution at the 50 and 100 community size, respectively. This extensive reduction is due to the demand to hold the investment for the insulation materials to sustain the SST performance in an acceptable range, and it will be reflected in the thermal performance of the SST.

Fig. 19 shows a comprehensive environmental breakdown for each component in the SDHS during its lifetime based on the *RCP* when applied at different community sizes under the FDV optimization setting. On the contrary to the environmental impact breakdown at the 10-buildings case, the Min. cost-optimal solution at the 25 buildings relays on renewable energy since the natural gas represents only 14.09% of the total impact. With the increment in the environmental damage limits, a progressive rise is indicated in the environmental impact due to introducing renewable energy components where the solar collector followed by the SST are the main contributors to the total environmental impact from scenario 2 to 5. With increasing the community size above 25 buildings, the environmental impact due to using natural extensively decrease where it represents only 13.9% and 9.60% in the Min. cost-optimal solution at the community size of 50 and 100 buildings, respectively.

In terms of the SST environmental impact, the construction material has the main contribution to the environmental impact of STT followed by the wall insulation material. It rises progressively with increasing the environmental damage limits, and it represents 32.1%, 23.1%, 23% and 18.7% for the community sizes of 10, 25, 50 and 100 building at the Min. optimal cost solution, this value increases to 99% at the Min. impact optimal solutions.

Following the energy analysis of the small urban community (10 buildings) located in Madrid, where the SST heat losses and its relative efficiency in addition to the solar fraction of the SH circuit are the key indicators in the SDHS, Fig. 20 shows the heat losses of the SST lining up with its coefficient under the PDV and FDV optimization setting at different community sizes. Under the PDV optimization setting, the

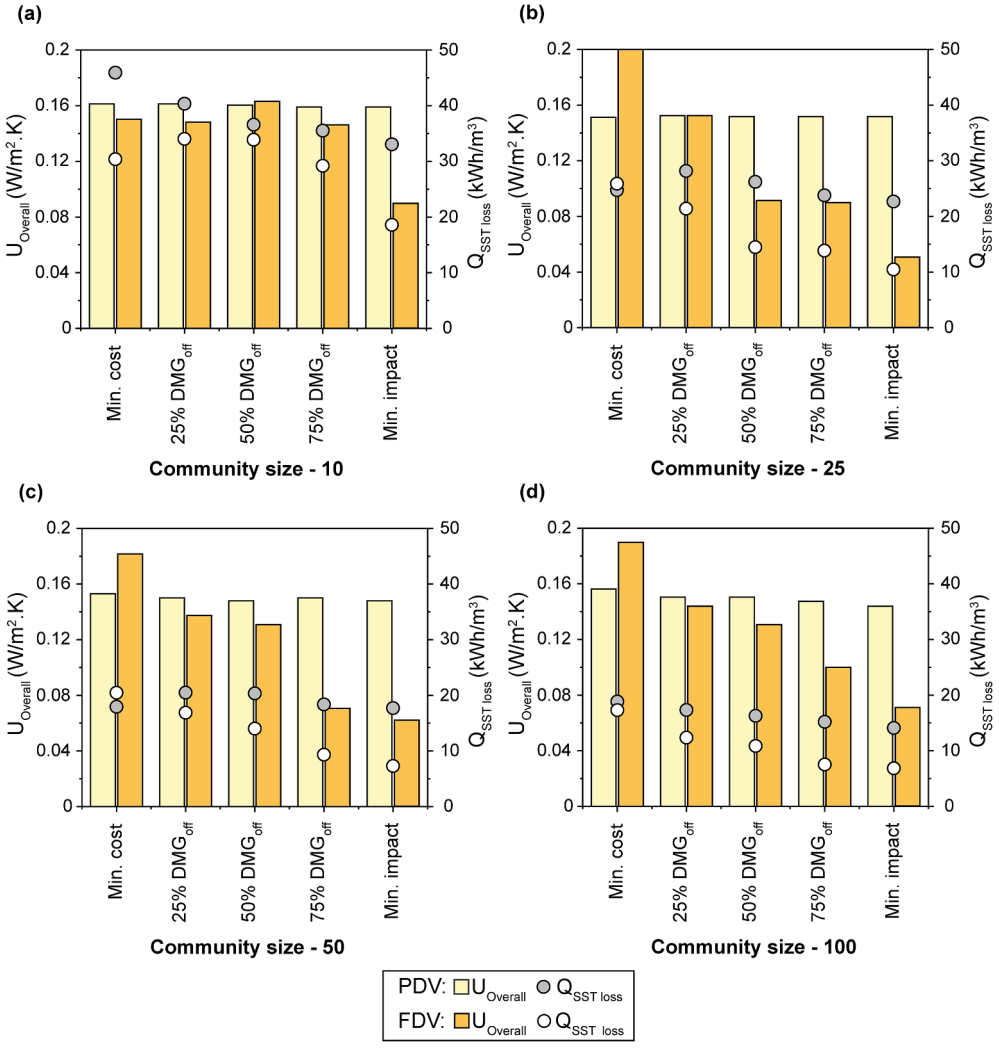

Fig. 20. Heat loss of the SST for the optimal Pareto SDHS solutions under PDV and FDV optimization settings. These designs satisfy the SH and DHW demand of different residential building sizes located in Madrid.

heat loss coefficient remains almost at 0.15 W/m^2·K for all scenarios at different community sizes. While the heat loss coefficient reduces progressively with increasing the environmental damage limits under the FDV optimization setting where the heat loss coefficient reduces from 0.2 W/m^2·K in scenario 1 (Min cost-optimal solution) to 0.05 W/m^2·K in scenario 5 (Min impact optimal solution) at the community size 25. In the community size of 50 and 100, the heat loss coefficient declines from 0.18 W/m^2·K to 0.05 W/m^2·K in the Min. cost and impact optimal solutions, respectively.

The privilege of reducing the heat loss coefficient due to introducing the SST construction materials in the optimization problem is reflected in the annual heat losses of the SST. Following the small community size of 10 buildings, the Min. cost-optimal solution under FDV optimization setting fails to improve the heat losses in the SST at the community size of 25 buildings where the heat losses of the SST is higher by 7.14% compared to the same scenario under the PDV optimization setting at community size of 25 buildings, respectively. While increasing the environmental damage limits, the heat losses in SST reduce progressively under the FDV optimization setting compared to its relative scenario under the PDV optimization setting where the SST heat losses reduced in the Min. impact optimal solution by 63.3%. The superiority of including the SST construction materials reveals in the community sizes of 50 and 100 at all optimal solutions except the Min. cost solution in the 50-community size where the SST heat losses increase by 15.8%. While in the community size of 100 buildings, the heat losses reduce by 11.8%. This improvement continues with increasing the environmental damage limits, and it is reduced by 58.2% and 52.3% for 50 and 100 buildings, respectively, at the min impact optimal solutions.

The improvement in the SST heat loss due to introducing the SST construction materials in the optimization problem can be mirrored in the η_{SST} and the solar fraction of the SH circuit, as shown in Fig. 21. In term of the η_{SST}, the SST efficiency rises with increasing the damage limits where the η_{SST} in the Min. cost optimal solution is 69.8%, 75.0%, and 78.9% for the community sizes of 25, 50, and 100 buildings, respectively. Moreover, this value increases in the Min. impact-optimal solutions to 87.8%, 90.4%, and 90.5% for the community size of 25, 50, and 100 buildings, respectively. Following the *S*. F_{SH} of the Min. cost optimal solution in the 10 building, a *S*. F_{SH} of 97.1% is indicated for a community size of 25 buildings. This value can be improved with the movement toward less environmental damage solution, and it achieves almost 100% in the Min. impact solution. With increasing the community size, a high *S*. F_{SH} is indicated in all optimal solution where a *S*. F_{SH} of 98% is indicated in the Min cost optimal solution, and it can reach almost 100% in the Min. impact optimal solution for both the 50 and 100 buildings.

5.3. Comparison of the optimal SDHS model to other projects

In this phase, our optimization framework results are compared with the results obtained by the framework proposed by Tulus et al. [38]. The main objective of this phase is to verify our optimization framework and indicate its advantage in enhancing the SDHS performance as well the computational expenses of the optimization process.

Aligning with the verification objective, the SDHS optimal solutions for a community size of 40 buildings located in Madrid is compared with Tulus et al. [38] results under an environmental damage of 50% scenario. The Tulus's framework considered only the solar collector field area and SST volume as decision variables in the optimization problem while the remain decision variables were fixed based on the Friedrichshafen project [126] for the SST construction materials. In addition, Tulus's setting was implemented in our framework to indicate the enhancement of including other decision variables as well as the SST construction properties in the optimization problem.

As shown in Table 7, our framework results using Tulus et al. [52] setting, which only considers the solar collector field and SST volume as decision variables in the optimization problem agrees with the optimal results obtained by Tulus et al. [38] article where the optimal size for the decision variables comprising the solar collector field and SST are almost identical in both cases. Furthermore, this verification extends to the performance indicators including the η_{DHWT}, S. F_{DHW} and S. F_{SH}. However, due to the low heat loss assumption in Tulus et al. [38] article for the SST, the heat loss coefficient is only 0.06 W/m^2·K, whereas in our optimization framework, where the SST construction materials were estimated based on the Friedrichshafen project [126], the heat loss coefficient is 0.15 W/m^2·K. This increment in the heat losses coefficient is reflected in the η_{SST} which is 81.2% compared to 96% in Tulus et al. [38]. Furthermore, the limitation in decision variables using our framework is reflected in the economic objective function where the *NPC* is 91.1 Euro/MWh. This extensive increment in the cost compared to Tulus et al. [38] is due to the usage of the mineral wool and Normal concert in the construction of the SST tank, and introducing the Auxiliary heaters with its full capacity as proposed in Tulus et al. [38]. On the other hand, the small cost of the SDHS in Tulus et al. [38] is due to estimating the SST cost as a function of the only its storage capacity without consideration for the cost of the SST construction materials.

After the verification stage, the developed methodology framework using the FDV optimization setting is tested against Tulus et al. [38] to approve the importance of including other decision variables comprising the SST properties in proposing a realistic estimation for the SDHS performance during its lifetime. The results under the FDV

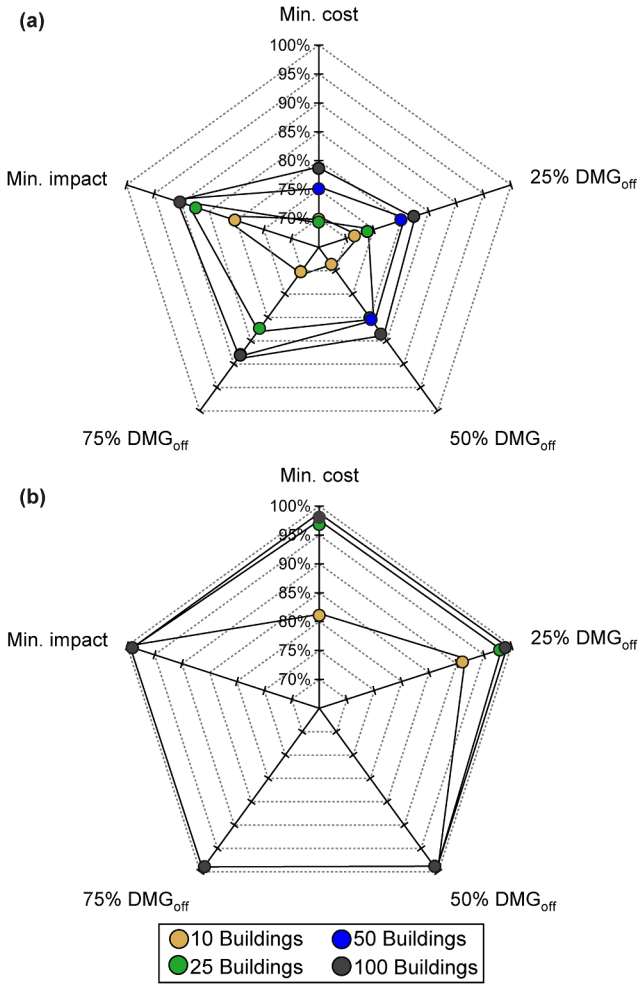

Fig. 21. The performance indicator including (a) η_{SST}, (B) *S*. F_{SH} for the optimal Pareto SDHS solutions under the FDV optimization settings at different community size.

Table 7
The Pareto optimal solution at environmental damage of 50% under different settings based on our simulation-optimization framework SDHS compared to Tulus et al. [38] results. This optimal solution covers SH and DHW demand of 40 buildings located in Madrid.

	Circuit Name			Tulus et al. [38]	Tulus setting using our framework	FDV optimization setting
Decision variables	Solar Circuit	Heat demand	(MWh/a)	7654	7654	7654
		A_{COL}	(m^2/MWh/a)	0.89	1.16	1.09
		β_{COL}		50	50	42.3
		N_{COL}		1	1	5
	SH circuit	V_{SST}	m^3/MWh/a	10	10.6	14.3
		HDR	m/m	0.6	0.6	0.75
		d_{Roof}	m	–	0.3	0.44
		d_{Wall}	m	–	0.2	0.30
		d_{Gnd}	m	–	0.2	0.13
		λ_{con}	W/m.K	–	NC	UHPC
		λ_{ins}	W/m.K	–	MW	XPS
		$\lambda_{ins\ gnd}$	W/m.K	–	MW	XPS
		FC_{AUX1}	–	1	1	0.66
	DHW Circuit	V_{DWHT}	m^3	109.7	109.9	177.8
		HDR_{DHWT}	m/m	1.7	1.7	1.35
		FC_{AUX2}	–	1	1	0.45
Main Performance indicators	DHW Circuit	η_{DHWT}	%	98.1	98.2	97.2
		S. F_{DHW}	%	98.9	98.8	99.8
	SH Circuit	$U_{Overall}$	W/m^2.K	0.06	0.15	0.09
		$Q_{SSTloss}$	kWh/m^3	3.11	21.6	12.4
		η_{SST}	%	96	81.2	85.3
		S. F_{SH}	%	97.8	96.3	99.9
	Economic indicators	*NPC*	Euro/MWh	53.3	91.1	58.5
	Environmental indicators	*RCP*	Pt/MWh	3.59	3.86	2.57

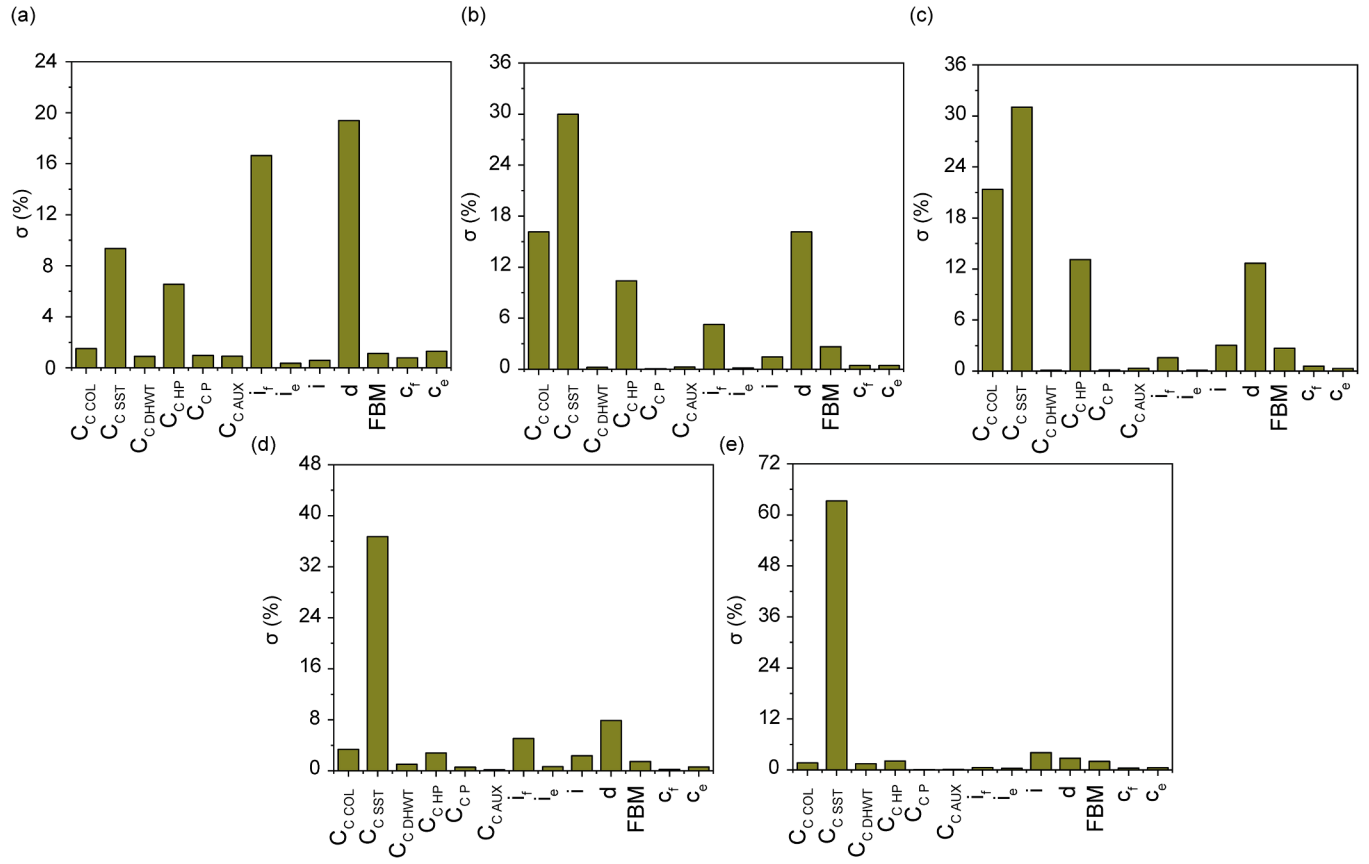

Fig. 22. Results of the BACCO analysis indicating the most influencing uncertain parameters with regards to the *NPC* under FDV optimization settings at different environmental damage scenarios where (a) Min. cost solution, (b) 25% damage off, (c) 50% damage off, (d) 75% damage off, (e) Min. impact solution.

optimization setting shift the SST size to 14.3 m^3/MWh/a with a slight difference in its aspect ratio where the HDR is 0.75 compared to 0.6 proposed in Tulus et al. [38]. The difference in the SST volume is reflected in the S. F_{DHW} and S. F_{SH} which are almost 100% for both circuits. Furthermore, our framework achieves this high renewable energy fractions without losing its efficiency due to the larger size for the SST, where the SST heat loss coefficient is 0.09 W/m^2·K. and the η_{SST} is around 85.3%. Moreover, including the FDV optimization setting is reflect in the economic and environmental indicators where the *NPC* is 58.5 Euro/MWh with an increment of 9.7% compared to Tulus et al. [38]. While the *RPC* under the FDV optimization setting is improved by the 28.4% due to including the SST material and construction properties.

In addition to the SDHS optimal solution comparison to Tulus et al. [38], the capability of the methodological optimization framework based on a robust ANN in handling the Heuristics optimization is illustrated through comparing the computational expenses of the optimization process with the SDHS optimization problem mentioned by Tulus et al. [38]. In Tulus et al. study, the average computation time for the anchor points was 15,700 CPU seconds and 47,000 CPU seconds for intermediate Pareto solutions using an Intel® Xeon® E5-2620 v4 2.10 GHz processor with 32.0 GB RAM. In this new framework, the average computational time for developing the full Pareto frontier is only around 600 CPU seconds using the same machine. This huge reduction is due to replacing the TRSNYS model with a robust ANN model and combining it in a MOO framework.

5.4. Global sensitivity analysis results

The GSA is implemented to identify the essential input parameters that responsible for the variation in both *NPC* and *RPC* objective functions. The analysis is carried out based on the BACCO analysis due to its low computational cost. The community of 10 buildings under the FDV optimization setting at different scenarios is selected as a reference case in the GSA due to its critical feasibility in comparison to the conventional system using natural gas. The evaluation assesses the economic parameters, including the investment cost of the SDHS equipment, the economic factors which would fasten the feasibility of SDHS deployment and the energy carriers. For the BACCO analysis, given a total number of 400 sample points based on the Latin hypercube sampling (LHS) design, the sensitivity analysis problem is formulated and feed into the Gaussian emulator machine sensitivity analysis (GEM-SA) software to perform the analysis.

The results of the BACCO analysis for economic performance is shown in Fig. 22. In each plot, the most influential parameters are ranked based on their variance contribution to the *NPC* objective function, and it represented through their total effect, which comprises the main effect, interactions between these parameters, and their high order terms that can be involved in the emulator model. In scenario 1 (Min. cost-optimal solution), the discount rate, followed by the annual natural gas inflation rate and the investment cost of the SST, are responsible for the greatest portion of the output variance. Moreover, a limited distribution for the renewable energy equipment is due to the dependency of the SDHS under scenario 1 on using natural gas. With the movement toward a lower environmental damage solution, the contribution of the initial investment cost of the SST increases with diminishing the contribution of the discount rate. In scenarios 2 and 3, the investment cost of the SST and the investment cost of the solar collector are the most influential parameters. While in scenarios 4 and 5, the investment cost of the SST is the only important uncertain parameter in designing SDHS. These results confirm the importance of including the SST construction materials, which can substantially

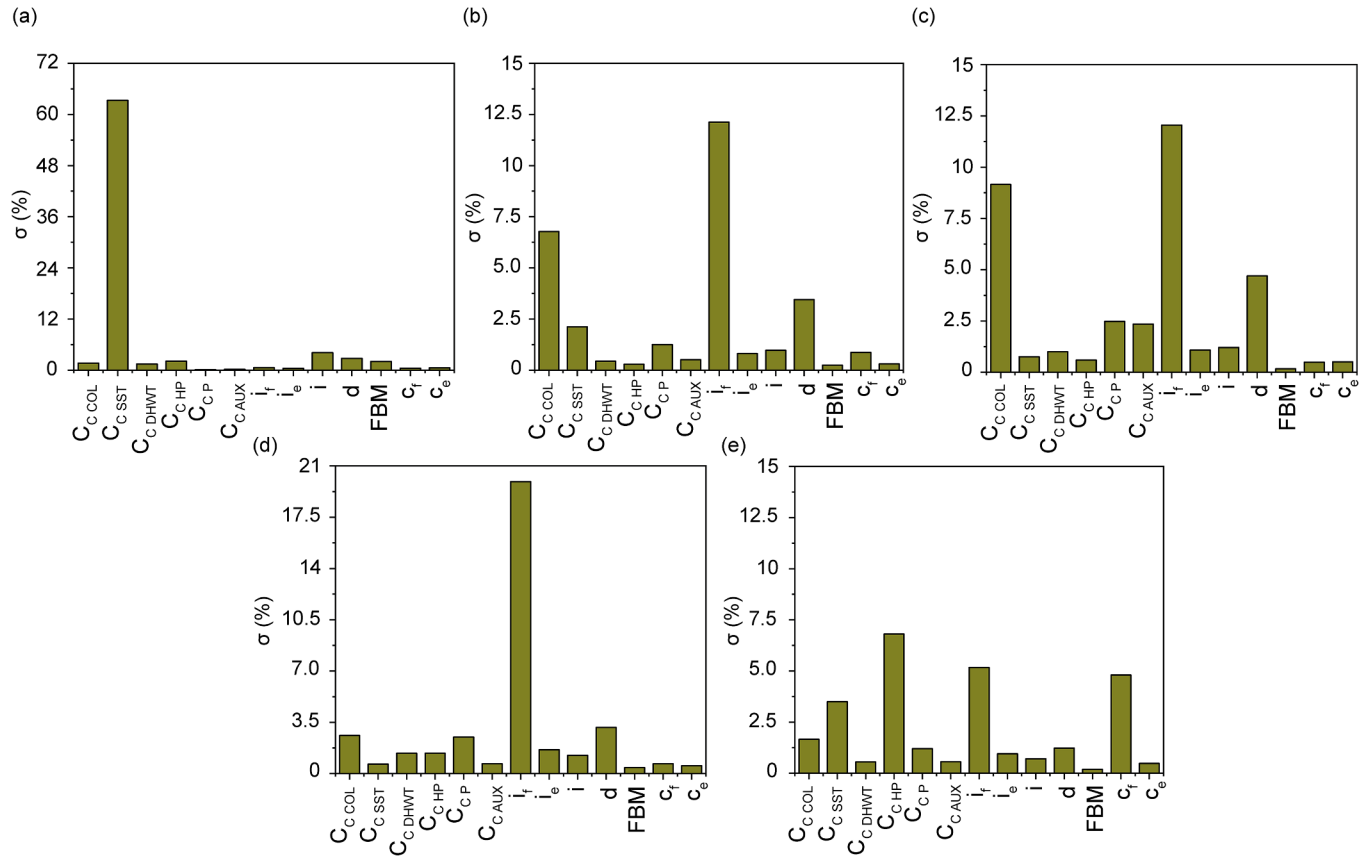

Fig. 23. Results of the BACCO analysis indicating the most influencing uncertain parameters with regards to the *RPC* under FDV optimization settings at different environmental damage scenarios where (a) Min. cost solution, (b) 25% damage off, (c) 50% damage off, (d) 75% damage off, (e) Min. impact solution.

improve the optimal solution and increase its competitivity against the conventional systems.

Following the sensitivity analysis for the economic performance of the SDHS based on BACCO analysis, Fig. 23 shows the sensitivity analysis for the *RPC* under different damage limits scenarios. In scenario 1, where the min possible change in the construction materials of the seasonal storage can be achieved due to the objective of minimizing the economic cost, the initial investment cost of the SST has the strongest influence in the *RPC* objective. With the possibly to change the construction materials due to increasing the environmental damage limits, the contribution of the investment cost of the SST starts to diminish, and the main contribution due to renewable energy equipment moves to the solar collector and natural gas. In scenarios 2 and 3, the annual natural gas inflation rate, followed by the investment cost of the solar collector field and discount rate, are the most influential parameters. While in scenario 4, the annual natural gas inflation rate appears to be the only relatively important parameter in this scenario. With moving toward the extensive environmental damage limit scenario (Min. impact solution), the investment cost of the heat exchangers followed by the annual natural gas inflation rate and the natural gas price represents the significant parameters that are affecting the *RPC* objective. Beside indicating the most influential parameters, the GSA based on BACCO analysis also indicates that the uncertainty due to the investment cost including the initial investment cost the DHWT, pumps and auxiliary heaters or due to the economic factors including the annual electricity inflation rate, inflation rate, and maintenance factor or due to the energy carrier including electricity prices can be neglected.

Overall, the GSA based on the BACCO analysis is a valuable decision-support technique that offers the SDHS designers valuable information regarding the main driver parameters of uncertainty. In the proposed case study, the construction materials of the SST and the annual natural gas inflation rate would, in return, significantly contribute to the *NPC* and *RPC* objective functions.

6. Conclusions

The Governance of the Energy Union ambitious plan to updates the EU energy policy framework concerning the sustainable transaction from fossil fuel toward the deployment of renewable energy encourages the widespread of methodologies that can quantify the renewable energy systems performance with consideration for its economic and environmental impact. This paper presents a framework to evaluate the feasibility of deploying the SDHS at different urban community sizes with tracing its techno-economic failures as well as its environmental impact. This methodology is implemented through developing a complete methodological optimization framework based on a robust ANN model to solve the computational obstacle associated with heuristics optimization models. The surrogate modelling approach empowers the feasibility of assessing the most influencing parameters driving the total cost of the SDHS based on GSA. The optimization framework correspondingly based on a multi-objective approach which is applied to optimize the SDHS life cycle cost with achieving progressively lower environmental impact throughout the system lifetime. In this context, the proposed framework is applied to four different urban community sizes comprising 10, 25, 50, and 100 buildings located in Madrid. In which the optimization problem is formulated under two different optimization settings (PDV and FDV) to investigate the effect of the seasonal TES geometry and its construction properties in enhancing the SDHS optimal design feasibility.

In the proposed framework, to overcome the ANN building computational barrier related to its design space exploration, and to optimize its tuning parameters (Hyperparameter), the ANN model is coupled with the Bayesian optimization approach assisted sensitivity analysis based on definitive screening. This procedure is utilized to develop a robust ANN model-independent on its hyperparameters and the training set size. Leading to create an accuracy ANN model that reflects the performance of the SDHS at affordable computational expenses, a summary of the robust ANN model key findings is the following:

- The default ANN model hyperparameters yield to poor accurate model that can predict the SDHS aggregated output. Thus, this result emphasizes the need for optimizing the hyperparameters.
- Relate to the ANN model settings, the hyperparameters comprising the number of hidden layers at 3, the number of neurons at 14, training function at Bayesian regularization, layer function at logsig, hidden function at purelin, learning rate at 0.001 and Momentum mean at 0.004 show the highest accurate ANN model at various training set size.
- Relate to the ANN model convergence at different training set sizes, the sample size of 2048 shows the highest accurate model prediction, where the $C.V$ criterion does not get below 5.3% for all model outputs at an affordable computational time of 8.9×10^3 sec.

Following the work objective in examining the effect of including the SST geometry and its construction material in enhancing the SDHS optimality when introduced at different urban community sizes. The following summarizes the key findings related to the MOO problem output under the PDV and FDV optimization setting in comparison to conventional heating systems using natural gas:

- The calculated Min. cost-optimal solutions demonstrate a progressive improvement in the economic and environment benefits for deploying SDHS instead of the natural gas boilers with the increment in the community sizes where the *NPC* is improved by 22%, 26.7%, 34.7% and 53.9% for community size of 10, 25, 50 and 100 buildings, respectively, under the PDV optimization setting. These values further improved with including the SST construction properties in the optimization problem (FDV setting) where the *NPC* is diminished more by 11.1%, 15.7%, 27.3% and 29.7% for community size of 10, 25, 50 and 100 buildings, respectively compared to its relative scenario under the PDV optimization settings. On the other hand, the extensive environmental solution (Min. impact solution) increases the *NPC* by 62.1%, 21.6% for the community size of 10, and 25 buildings, respectively, in comparison to the conventional system using natural gas. While increasing the community size to 50 and 100 buildings, increases the competitively of the SDHS, where the *NPC* is reduced by 2.13% and 19.7% for 50 and 100 buildings, respectively. With running the optimization problem under the FDV settings, further investment is required compared to the optimization problem under PDV setting where the *NPC* is increased by 13.4%, 21.6%, 20.8% and 1.84% for the community size of 10, 25, 50 and 100 building, respectively. This increment is due to the considerable reduction in the environmental impact for the FDV optimal solutions compared to its relative solutions under the PDV setting.
- In terms of the environmental benefits for deploying SDHS at different urban community sizes, the *RPC* at the Min. cost-optimal solution is reduced by 79.4%, 79.5%, 79.6%, and 79.7% for the community size of 10, 25, 50, and 100 buildings, respectively under the PDV setting in comparison to the natural gas boilers. Under the FDV optimization setting, a progressive improvement in the *RPC* is indicated with increasing the community size where the *RPC* is diminished more by 0.27%, 39.07%, 43%, and 47.7% for community size of 10, 25, 50 and 100 building compared to its relative solution under PDV setting. Moreover, with the movement toward an environmental solution, the improvement in the*RPC* is increased, and it achieved 88% in the community size of 100 building under the PDV setting, this improvement can be more extensive under the FDV setting where it reduced up 27.3% compared to its relative solution under the PDV setting.
- The effect of including the SST material properties in the

optimization problem is reflected in the economic and environmental payback period where the EPBP at the Min. cost optimal-solution is reduced from 33.3 years at community size of 10–13.7 years at the community size of 100 buildings under the FDV setting. While the GPBP is only around 4 years for the Min. impact solutions at different community sizes.

- Aligning with tracing the technical failure of the SST in the optimization framework, the optimal solutions under the FDV settings show an extensive improvement in the SST heat loss. This improvement is increased with the increment in the environmental damage limits, and it varies between 18.5 and 6.9 kWh/m^3 for community sizes 10 and 100 buildings. This reduction in the heat losses is reflected in the SST efficiency where all optimal solution at different community sizes never falls below 69.5% in the Min. cost-optimal solution, and it extends up to 90.5% at the Min. impact-optimal solution at community size of 100 building. Furthermore, the yearly solar fraction never falls below 82.1% for the investigated community sizes, and it expands to almost 100% in the high environmental damage limits scenarios.
- Finally, the GSA based on the BACCO analysis reveals that the variation in the optimal SDHS cost and its relative impact is due to the initial investment cost of the SST and its relevant construction materials in addition to the annual natural gas inflation rate. In contrast, the rest of the uncertain parameters have a limited influence.

In the real application of designing the SDHS, the present methodology can be beneficial to obtain the optimal sizing of the renewable energy equipment with consideration for the construction properties of the SST, and it initiates values of 1.1 ± 0.1 m^2/MWh/a and 15 ± 1 m^3/MWh/a for the solar collector field area and the SST volume, respectively at different community sizes. Furthermore, the proposed framework provokes the superiority of using the UHPC in the construction of SST and FG for insulation. These guiding can serve all project stakeholders to participate in the early design phases or developing business models for the SDHS.

The proposed framework can provide a good starting point to cover the drawbacks associated with the surrogate modeling technique and solve the enormous computational expenses of the heuristics optimization approach. Moreover, it is an effective tool to evaluate the techno-economic performance of the SDHS as well its environmental benefits with consideration for the market fluctuation regarding the investment cost and the energy carriers. Furthermore, it can assist in proposing the SDHS as a competitive solution instead of the conventional heating systems, and subsequently, it can promote a clear statement regarding the new clean energy for all Europeans packages.

CRediT authorship contribution statement

Mohamed Hany Abokersh: Conceptualization, Methodology, Investigation, Formal analysis, Software, Data curation, Visualization, Writing - original draft. **Manel Vallès:** Conceptualization, Writing - review & editing, Supervision. **Luisa F. Cabeza:** Funding acquisition, Writing - review & editing. **Dieter Boer:** Resources, Supervision, Writing - review & editing, Project administration.

Declaration of Competing Interest

The authors declared that there is no conflict of interest.

Acknowledgments

The work is funded by the Spanish government RTI2018-093849-B-C31 and RTI2018-093849-B-C33. The authors would like to thank the Catalan Government for the quality accreditation given to their research group (GREiA - 2017 SGR 1537, AGACAPE - 2017 SGR 1409). GREiA is a certified agent TECNIO in the category of technology developers from the Government of Catalonia. This work is partially supported by ICREA under the ICREA Academia programme. This work is partially funded by the Ministerio de Ciencia, Innovación y Universidades – Agencia Estatal de Investigación (AEI) (RED2018-102431-T). This project has received funding from the European Union's Horizon 2020 research and innovation programme under the Marie Skłodowska-Curie grant agreement No. 713679 and from the Universitat Rovira i Virgili (URV).

References

[1] International Renewable Energy Agency (IRENA). Global energy transformation: a roadmap to 2050; 2018.
[2] European Commission. Clean energy for all Europeans. Luxembourg; 2019. doi: 10.2833/9937.
[3] European Commission. Communication from the commission to the European Parliament and the Council. Brussels; 2016.
[4] European Energy Agency. Final energy consumption by sector and fuel; 2015. doi: CSI 027/ENER 016.
[5] Balaras CA, Gaglia AG, Georgopoulou E, Mirasgedis S, Sarafidis Y, Lalas DP. European residential buildings and empirical assessment of the Hellenic building stock, energy consumption, emissions and potential energy savings. Build Environ 2007;42:1298–314. https://doi.org/10.1016/j.buildenv.2005.11.001.
[6] Eurostat. Final energy consumption in the residential sector by type of end-use; 2016. https://ec.europa.eu/eurostat/statistics-explained/index.php?title=File:Final_energy_consumption_in_the_residential_sector_by_type_of_end-use,_EU-28,_2015.png&oldid=340063 [accessed June 27, 2019].
[7] European Environment Agency. Annual European Union greenhouse gas inventory 1990–2017 and inventory report 2019; 2019. doi: 10.2800/41819.
[8] European Commission (Directive 2010/31/EC). On the energy performance of buildings; 2012.
[9] Antoniadis CN, Martinopoulos G. Optimization of a building integrated solar thermal system with seasonal storage using TRNSYS. Renew Energy 2019;137:56–66. https://doi.org/10.1016/j.renene.2018.03.074.
[10] Rad FM, Fung AS. Solar community heating and cooling system with borehole thermal energy storage - review of systems. Renew Sustain Energy Rev 2016;60:1550–61. https://doi.org/10.1016/j.rser.2016.03.025.
[11] Carrilho da Graça G, Augusto A, Lerer MM. Solar powered net zero energy houses for southern Europe: feasibility study. Sol Energy 2012;86:634–46. https://doi.org/10.1016/j.solener.2011.11.008.
[12] Gao L, Zhao J, Tang Z. A review on borehole seasonal solar thermal energy Storage. Energy Proc 2015;70:209–18. https://doi.org/10.1016/j.egypro.2015.02.117.
[13] Cabeza LF, Martorell I, Miró L, Fernández AI, Barreneche C. Introduction to thermal energy storage (TES) systems. Woodhead Publishing Limited; 2014. doi: 10.1533/9781782420965.1.
[14] Dahash A, Ochs F, Janetti MB, Streicher W. Advances in seasonal thermal energy storage for solar district heating applications: a critical review on large-scale hot-water tank and pit thermal energy storage systems. Appl Energy 2019;239:296–315. https://doi.org/10.1016/j.apenergy.2019.01.189.
[15] Li Q, Tehrani SSM, Taylor RA. Techno-economic analysis of a concentrating solar collector with built-in shell and tube latent heat thermal energy storage. Energy 2017;121:220–37. https://doi.org/10.1016/j.energy.2017.01.023.
[16] International Renewable Energy Agency (IRENA). The Energy Technology Systems Analysis Programme (ESTAP): technology brief E17; 2013.
[17] Reed AL, Novelli AP, Doran KL, Ge S, Lu N, McCartney JS. Solar district heating with underground thermal energy storage: pathways to commercial viability in North America. Renew Energy 2018;126:1–13. https://doi.org/10.1016/j.renene.2018.03.019.
[18] Xu J, Wang RZ, Li Y. A review of available technologies for seasonal thermal energy storage. Sol Energy 2014;103:610–38. https://doi.org/10.1016/j.solener.2013.06.006.
[19] Reuss M. Advances in thermal energy storage systems: methods and applications. United Kingdom: Woodhead Publishing Limited; 2015.
[20] Bankston CA. The status and potential of central solar heating plants with seasonal storage: an international Report. Adv Sol Energy. New York: Plenum Press; 1988. p. 352–444.
[21] Tian Z, Perers B, Furbo S, Fan J. Thermo-economic optimization of a hybrid solar district heating plant with flat plate collectors and parabolic trough collectors in series. Energy Convers Manag 2018;165:92–101. https://doi.org/10.1016/j.enconman.2018.03.034.
[22] Bauer D, Marx R, Nußbicker-Lux J, Ochs F, Heidemann W, Müller-Steinhagen H. German central solar heating plants with seasonal heat storage. Sol Energy 2010;84:612–23. https://doi.org/10.1016/j.solener.2009.05.013.
[23] Rehman ur H, Hirvonen J, Sirén K. Influence of technical failures on the performance of an optimized community-size solar heating system in Nordic conditions. J Clean Prod 2018;175:624–40. https://doi.org/10.1016/j.jclepro.2017.12.088.
[24] Urbaneck T, Oppelt T, Platzer B, Frey H, Uhlig U, Göschel T, et al. Solar district heating in east Germany - transformation in a cogeneration dominated city. Energy Proc 2015;70:587–94. https://doi.org/10.1016/j.egypro.2015.02.164.

[25] BINE Information Service. Solar-assisted District Heating [Online]; 2000.
[26] Sibbitt B, McClenahan D, Djebbar R, Thornton J, Wong B, Carriere J, et al. The performance of a high solar fraction seasonal storage district heating system - Five years of operation. Energy Proc 2012;30:856–65. https://doi.org/10.1016/j.egypro.2012.11.097.
[27] Sibbit B, McClenahan D, Djebbar R, Paget K. GroundBreaking Solar. vol. Summer. Canada; 2015.
[28] Weissmann C, Hong T, Graubner CA. Analysis of heating load diversity in German residential districts and implications for the application in district heating systems. Energy Build 2017;139:302–13. https://doi.org/10.1016/j.enbuild.2016.12.096.
[29] Yang Y, Zhang S, Xiao Y. Optimal design of distributed energy resource systems coupled withenergy distribution networks. Energy 2015;85:433–48. https://doi.org/10.1016/j.energy.2015.03.101.
[30] Gonzalez-Garay A, Guillen-Gosalbez G. SUSCAPE: A framework for the optimal design of SUStainable ChemicAl ProcEsses incorporating data envelopment analysis. Chem Eng Res Des 2018;137:246–64. https://doi.org/10.1016/j.cherd.2018.07.009.
[31] Klatt KU, Marquardt W. Perspectives for process systems engineering-Personal views from academia and industry. Comput Chem Eng 2009;33:536–50. https://doi.org/10.1016/j.compchemeng.2008.09.002.
[32] Buoro D, Pinamonti P, Reini M. Optimization of a distributed cogeneration system with solar district heating. Appl Energy 2014;124:298–308. https://doi.org/10.1016/j.apenergy.2014.02.062.
[33] Welsch B, Göllner-Völker L, Schulte DO, Bär K, Sass I, Schebek L. Environmental and economic assessment of borehole thermal energy storage in district heating systems. Appl Energy 2018;216:73–90. https://doi.org/10.1016/j.apenergy.2018.02.011.
[34] Skiborowski M, Rautenberg M, Marquardt W. A hybrid evolutionary-deterministic optimization approach for conceptual design. Ind Eng Chem Res 2015;54:10054–72. https://doi.org/10.1021/acs.iecr.5b01995.
[35] Rehman ur H, Hirvonen J, Sirén K. Performance comparison between optimized design of a centralized and semi-decentralized community size solar district heating system. Appl Energy 2018;229:1072–94. https://doi.org/10.1016/j.apenergy.2018.08.064.
[36] Tulus V, Boer D, Cabeza LF, Jiménez L, Guillén-Gosálbez G. Enhanced thermal energy supply via central solar heating plants with seasonal storage: a multi-objective optimization approach. Appl Energy 2016;181:549–61. https://doi.org/10.1016/j.apenergy.2016.08.037.
[37] Bava F, Furbo S. Development and validation of a detailed TRNSYS-Matlab model for large solar collector fields for district heating applications. Energy 2017;135:698–708. https://doi.org/10.1016/j.energy.2017.06.146.
[38] Tulus V, Abokersh MH, Cabeza LF, Vallès M, Jiménez L, Boer D. Economic and environmental potential for solar assisted central heating plants in the EU residential sector: contribution to the 2030 climate and energy EU agenda. Appl Energy 2019. https://doi.org/10.1016/j.apenergy.2018.11.094.
[39] Ciampi G, Rosato A, Sibilio S. Thermo-economic sensitivity analysis by dynamic simulations of a small Italian solar district heating system with a seasonal borehole thermal energy storage. Energy 2018;143:757–71. https://doi.org/10.1016/j.energy.2017.11.029.
[40] Saltelli A, Annoni P. How to avoid a perfunctory sensitivity analysis. Environ Model Softw 2010;25:1508–17. https://doi.org/10.1016/j.envsoft.2010.04.012.
[41] Mavromatidis G, Orehounig K, Carmeliet J. Uncertainty and global sensitivity analysis for the optimal design of distributed energy systems. Appl Energy 2018;214:219–38. https://doi.org/10.1016/j.apenergy.2018.01.062.
[42] Bornatico R, Hüssy J, Witzig A, Guzzella L. Surrogate modeling for the fast optimization of energy systems. Energy 2013;57:653–62. https://doi.org/10.1016/j.energy.2013.05.044.
[43] Wong SL, Wan KKW, Lam TNT. Artificial neural networks for energy analysis of office buildings with daylighting. Appl Energy 2010;87:551–7. https://doi.org/10.1016/j.apenergy.2009.06.028.
[44] Yaïci W, Entchev E. Performance prediction of a solar thermal energy system using artificial neural networks. Appl Therm Eng 2014;73:1348–59. https://doi.org/10.1016/j.applthermaleng.2014.07.040.
[45] Xia L, Ma Z, Kokogiannakis G, Wang Z, Wang S. A model-based design optimization strategy for ground source heat pump systems with integrated photovoltaic thermal collectors. Appl Energy 2018;214:178–90. https://doi.org/10.1016/j.apenergy.2018.01.067.
[46] Wang Z, Srinivasan RS. A review of artificial intelligence based building energy use prediction: contrasting the capabilities of single and ensemble prediction models. Renew Sustain Energy Rev 2017;75:796–808. https://doi.org/10.1016/j.rser.2016.10.079.
[47] Bauer D, Marx R, Drück H. Solar district heating for the built environment technology and future trends within the European project Einstein. Energy Proc 2014;57:2716–24. https://doi.org/10.1016/j.egypro.2014.10.303.
[48] Hirvonen J, Ur Rehman H, Sirén K. Techno-economic optimization and analysis of a high latitude solar district heating system with seasonal storage, considering different community sizes. Sol Energy 2018;162:472–88. https://doi.org/10.1016/j.solener.2018.01.052.
[49] Klein SA et al. TRNSYS Version. 18, Solar Energy Laboratory, University of Wisconsin-Madison; 2004. Website: < http://sel.me.wisc.edu/trnsys > .
[50] Guillén-gosálbez G, Grossmann I. A global optimization strategy for the environmentally conscious design of chemical supply chains under uncertainty in the damage assessment model 2010;34:42–58. doi: 10.1016/j.compchemeng.2009.09.003.
[51] De Guadalfajara M, Lozano MA, Serra LM. Evaluation of the potential of large solar heating plants in Spain. Energy Proc 2012;30:839–48. https://doi.org/10.1016/j.egypro.2012.11.095.
[52] Østergård T, Jensen RL, Maagaard SE. A comparison of six metamodeling techniques applied to building performance simulations. Appl Energy 2018;211:89–103. https://doi.org/10.1016/j.apenergy.2017.10.102.
[53] Bhosekar A, Ierapetritou M. Advances in surrogate based modeling, feasibility analysis, and optimization: a review. Comput Chem Eng 2018;108:250–67. https://doi.org/10.1016/j.compchemeng.2017.09.017.
[54] Wang GG, Shan S. Review of metamodeling techniques in support of engineering design optimization. J Mech Des 2007;129:370. https://doi.org/10.1115/1.2429697.
[55] Kucherenko S, Albrecht D, Saltelli A. Exploring multi-dimensional spaces: a Comparison of Latin Hypercube and Quasi Monte Carlo Sampling Techniques. 8th IMACS Semin. Monte Carlo methods; 2015. p. 1–32. doi: 10.1016/j.ress.2017.04.003.
[56] Robinson C, Dilkina B, Hubbs J, Zhang W, Guhathakurta S, Brown MA, et al. Machine learning approaches for estimating commercial building energy consumption. Appl Energy 2017;208:889–904. https://doi.org/10.1016/j.apenergy.2017.09.060.
[57] Carpenter J, Woodbury KA, O'Neill Z. Using change-point and Gaussian process models to create baseline energy models in industrial facilities: a comparison. Appl Energy 2018;213:415–25. https://doi.org/10.1016/j.apenergy.2018.01.043.
[58] Huang CL, Chen MC, Wang CJ. Credit scoring with a data mining approach based on support vector machines. Expert Syst Appl 2007;33:847–56. https://doi.org/10.1016/j.eswa.2006.07.007.
[59] Lin SW, Ying KC, Chen SC, Lee ZJ. Particle swarm optimization for parameter determination and feature selection of support vector machines. Expert Syst Appl 2008;35:1817–24. https://doi.org/10.1016/j.eswa.2007.08.088.
[60] Xia Y, Liu C, Li YY, Liu N. A boosted decision tree approach using Bayesian hyperparameter optimization for credit scoring. Expert Syst Appl 2017;78:225–41. https://doi.org/10.1016/j.eswa.2017.02.017.
[61] Snoek J, Larochelle H. Practical Bayesian optimization of machine learning algorithms. Adv Neural Inf Process Syst 2012:2951–9. https://doi.org/10.1016/S2468-2667(17)30214-1.
[62] Wiese M, Runge-borchert G, Raatz A. Optimization of neural network hyperparameters for modeling of soft pneumatic actuators. New Trends Med Serv Robot, vol. 48, Springer International Publishing; 2019, p. 199–206. doi: 10.1007/978-3-319-59972-4.
[63] Bergstra J, Yamins D, Cox DD. Hyperopt: a python library for optimizing the hyperparameters of machine learning algorithms. Proc 12th Python Sci Conf 2013:13–20.
[64] Jones B, Nachtsheim CJ, Jones B. A class of screening designs robust to active second-order effects a class of three-level designs for definitive screening in the presence of second-order effects. J Qual Technol 2011;43:1–15. https://doi.org/10.1007/978-3-7908-2410-0.
[65] Montgomery DC. Design and analysis of experiments, 8th ed. John Wiley & Sons, Inc.; 2013.
[66] Amasyali K, El-gohary NM. A review of data-driven building energy consumption prediction studies 2018;81:1192–205. doi: 10.1016/j.rser.2017.04.095.
[67] Guadalfajara M, Lozano MA, Serra LM. Analysis of large thermal energy storage for solar district heating. Eurotherm Semin #99 Adv Adv Therm Energy Storage 2014. https://doi.org/10.13140/2.1.3857.6008.
[68] Chung M, Park J, Yoon H. Simulation of a central solar heating system with seasonal storage in Korea. Sol Energy 1998;64:163–78.
[69] Hobbi A, Siddiqui K. Optimal design of a forced circulation solar water heating system for a residential unit in cold climate using TRNSYS. Sol Energy 2009;83:700–14. https://doi.org/10.1016/j.solener.2008.10.018.
[70] Hui L, Edem NTK, Nolwenn LP, Lingai L. Evaluation of a seasonal storage system of solar energy for house heating using different absorption couples. Energy Convers Manag 2011;52:2427–36. https://doi.org/10.1016/j.enconman.2010.12.049.
[71] Hang Y, Qu M, Ukkusuri S. Optimizing the design of a solar cooling system using central composite design techniques. Energy Build 2011;43:988–94. https://doi.org/10.1016/j.enbuild.2010.12.024.
[72] Allouhi A, Agrouaz Y, Benzakour Amine M, Rehman S, Buker MS, Kousksou T, et al. Design optimization of a multi-temperature solar thermal heating system for an industrial process. Appl Energy 2017;206:382–92. https://doi.org/10.1016/j.apenergy.2017.08.196.
[73] Kalogirou SA. Solar energy engineering: processes and systems. 1st ed. Academic Press; 2009. 10.1016/B978-0-12-374501-9.00014-5.
[74] Ximenes A, Barreneche C, Fernández AI, Cabeza LF. Life cycle costing as a bottom line for the life cycle sustainability assessment in the solar energy sector: a review. Sol Energy 2018. https://doi.org/10.1016/j.solener.2018.04.011.
[75] Gluch P, Baumann H. The life cycle costing (LCC) approach: a conceptual discussion of its usefulness for environmental decision-making. Build Environ 2004;39:571–80. https://doi.org/10.1016/j.buildenv.2003.10.008.
[76] Vikas K, Cheshta K, Savita N, Baredar P. Prefeasibility assessment of a tidal energy system. Tidal Energy Syst. Des. Optim. Control, Elsevier 2019:115–88. https://doi.org/10.1016/B978-0-12-814881-5.00003-X.
[77] Guillén-Gosálbez G, Caballero JA, Jiménez L. Application of life cycle assessment to the structural optimization of process flowsheets. Ind Eng Chem Res 2008;47:777–89. https://doi.org/10.1016/S1570-7946(07)80218-5.
[78] Nemerow NL, Agardy FJ, Sullivan P, Salvato JA. Environmental engineering: environmental health and safety for municipal infrastructure, land use and planning, and industry. 6th ed. John Wiley & Sons, Inc; 2009.
[79] ISO/TC 207/SC 5. ISO 14040:2006 Environmental management — Life cycle assessment — Principles and framework; 2006.
[80] International Organization for Standardization (ISO). ISO 14041: Environmental

Management - Life Cycle Assessment: Goal and Scope Definition and Inventory Analysis; 1997.
[81] International Organization for Standardization (ISO). ISO 14042: Environmental management - Life cycle assessment - Life cycle impact; 2000.
[82] Ecoinvent. Eco invent; 2017. https://www.ecoinvent.org/home.html [accessed March 12, 2018].
[83] JRC European commission (JRC-IES). ILCD Handbook: Recommendations for Life Cycle Impact Assessment in the European context. 1st ed. Luxemburg: Office of the European Union; 2011. doi: 10.278/33030.
[84] Li DHW, Lam TNT, Chan WWH, Mak AHL. Energy and cost analysis of semi-transparent photovoltaic in office buildings. Appl Energy 2009;86:722–9. https://doi.org/10.1016/j.apenergy.2008.08.009.
[85] Lu L, Yang HX. Environmental payback time analysis of a roof-mounted building-integrated photovoltaic (BIPV) system in Hong Kong. Appl Energy 2010;87:3625–31. https://doi.org/10.1016/j.apenergy.2010.06.011.
[86] Solites. Guideline for seasonal thermal energy storage systems in the built environment. Stuttgart; 2016.
[87] Ehrgott M. Multicriteria optimization. Heidelberg: Springer; 2005.
[88] Deb K. Multiobjective optimization using evolutionary algorithms. New York, NY: John Wiley & Sons, Inc; 2001.
[89] Konak A, Coit DW, Smith AE. Multi-objective optimization using genetic algorithms: a tutorial. Reliab Eng Syst Saf 2006;91:992–1007. https://doi.org/10.1016/j.ress.2005.11.018.
[90] Dalenbäck J-OG. Large-scale solar heating; 1999.
[91] Rehman ur H, Hirvonen J, Sirén K. A long-term performance analysis of three different configurations for community-sized solar heating systems in high latitudes. Renew Energy 2017;113:479–93. https://doi.org/10.1016/j.renene.2017.06.017.
[92] Li X, Liu M, Duanmu L, Ji Y. The optimization of solar heating system with seasonal storage based on a real project. Proc Eng 2015;121:1341–8. https://doi.org/10.1016/j.proeng.2015.09.017.
[93] Argiriouf A. CSHPSS systems in Greece : test of simulation and analysis of typical systems software 1997;60:159–70.
[94] Tao T, Zhang F, Zhang W, Wan P, Shen X, Li H. Low cost and marketable operational experiences for a solar heating system with seasonal thermal energy storage (SHSSTES) in Hebei. Energy Proc 2015;70:267–74. https://doi.org/10.1016/j.egypro.2015.02.123.
[95] Shahedan NF, Mustafa M, Bakri A. Review on thermal insulation performance in various type of concrete. AIP Conf Proc, AIP Publishing 2017:1–6. https://doi.org/10.1063/1.4981868.
[96] Reineck K, Prof A, Lichtenfels A, Engineers L. Concrete hot water tanks for solar energy storage; 2004.
[97] Reineck K, Greiner S, Reinhardt H. Dichte Heißwasser-Wärmespeicher aus ultrahochfestem Faserfeinkornbeton. Stuttgart 2004.
[98] Oliveti G, Arcuri N. Prototype experimental plant for the interseasonal storage of solar energy for the winter heating of buildings: description of plant and its functions. Sol Energy 1995;54:85–97.
[99] Hesaraki A, Halilovic A, Holmberg S. Low-temperature heat emission combined with seasonal thermal storage and heat pump. Sol Energy 2015;119:122–33. https://doi.org/10.1016/j.solener.2015.06.046.
[100] Deb K, Pratap A, Agarwal S, Meyarivan TAMT. A fast and elitist multiobjective genetic algorithm: NSGA-II. IEEE Trans Evol Comput 2002;6:182–97. doi: 10.1109/4235.996017.
[101] ur Rehman Hassam, Hirvonen Janne, Sirén Kai. Performance comparison between optimized design of a centralized and semi-decentralized community size solar district heating system. Appl Energy 2018;229:1072–94. https://doi.org/10.1016/j.apenergy.2018.08.064.
[102] Alajmi A, Wright J. Selecting the most efficient genetic algorithm sets in solving unconstrained building optimization problem. Int J Sustain Built Environ 2014;3:18–26. https://doi.org/10.1016/j.ijsbe.2014.07.003.
[103] Kennedy MC, O'Hagan A. Bayesian calibration of computer models. J R Stat Soc Ser B (Statistical Methodol) 2001;63:425–64. https://doi.org/10.1111/1467-9868.00294.
[104] Uusitalo L, Lehikoinen A, Helle I, Myrberg K. An overview of methods to evaluate uncertainty of deterministic models in decision support. Environ Model Softw 2015;63:24–31. https://doi.org/10.1016/j.envsoft.2014.09.017.
[105] Petropoulos G, Wooster MJ, Carlson TN, Kennedy MC, Scholze M. A global Bayesian sensitivity analysis of the 1d SimSphere soil-vegetation-atmospheric transfer (SVAT) model using Gaussian model emulation. Ecol Modell 2009;220:2427–40. https://doi.org/10.1016/j.ecolmodel.2009.06.006.
[106] Institute for Energy Diversification and Saving - IDAE. Análisis del consumo energético del sector residencial en España. INFORME FINAL; 2011.
[107] Guadalfajara M. Evaluación de centrales solares térmicas con acumulación estacional para el sector residencial en España 2013. https://doi.org/10.1017/CBO9781107415324.004.
[108] Pahud D. Central solar heating plants with seasonal duct storage and short-term water storage: design guidelines obtained by dynamic system simulations. Sol Energy 2000;69:495–509. https://doi.org/10.1016/S0038-092X(00)00119-5.
[109] United Nations Environment Programme, Solar Thermal Energy Technology Fact Sheet; 2014.
[110] U.S. Department of Energy. EnergyPlus. Energy simulation software: weather data n.d.; 2015.
[111] Trimble. SketchUp; 2012. http://www.sketchup.com.
[112] Jordan U, Vajen K. DHWcalc: program to generate domestic hot water profiles with statistical means for user defined conditions. Proc ISES Sol World Congr, Orlando (US): n.d. p. 8–12.
[113] European Commision. EuroStat; 2018. http://ec.europa.eu/eurostat/web/energy/data/database [accessed March 12, 2018].
[114] Braungardt S, Eichhammer W, Elsland R, Fleiter T, Klobasa M, Krail M, et al. Study evaluating the current energy efficiency policy framework in the EU and providing orientation on policy options for realising the cost-effective energy-efficiency/saving potential until 2020 and beyond; 2014.
[115] Ellehauge K, Pedersen T. Solar heat storages in district heating networks. Energinet.dk, PREHEAT project no. 2006-2-6750; 2007.
[116] Schmidt T, Mangold D. Status of solar thermal seasonal storage in Germany; 2009.
[117] Calise F, Dentice d'Accadia M, Palombo A. Transient analysis and energy optimization of solar heating and cooling systems in various configurations. Sol Energy 2010;84:432–49. https://doi.org/10.1016/j.solener.2010.01.001.
[118] austrotherm. General price list; 2017. doi: 10.5962/bhl.title.138707.
[119] Specialist Insulation Supplies Ltd. Prices list; 2018.
[120] GLAPOR-Schaumglasprodukte. GLAPOR PRICE LIST. Belgium; 2014.
[121] Aven T. Interpretations of alternative uncertainty representations in a reliability and risk analysis context. Reliab Eng Syst Saf 2011;96:353–60. https://doi.org/10.1016/j.ress.2010.11.004.
[122] Burhenne S, Tsvetkova O, Jacob D, Henze GP, Wagner A. Uncertainty quantification for combined building performance and cost-benefit analyses. Build Environ 2013;62:143–54. https://doi.org/10.1016/j.buildenv.2013.01.013.
[123] Mirkhani S, Saboohi Y. Stochastic modeling of the energy supply system with uncertain fuel price - A case of emerging technologies for distributed power generation. Appl Energy 2012;93:668–74. https://doi.org/10.1016/j.apenergy.2011.12.099.
[124] Mavrotas G, Florios K, Vlachou D. Energy planning of a hospital using Mathematical Programming and Monte Carlo simulation for dealing with uncertainty in the economic parameters. Energy Convers Manag 2010;51:722–31. https://doi.org/10.1016/j.enconman.2009.10.029.
[125] Bustos F, Toledo A, Contreras J, Fuentes A. Sensitivity analysis of a photovoltaic solar plant in Chile. Renew Energy 2016;87:145–53. https://doi.org/10.1016/j.renene.2015.09.070.
[126] Bauer D, Marx R, Nußbicker-Lux J. German central solar heating plants with seasonal heat storage. Sol Energy 2010;84:612–23. https://doi.org/10.1016/j.solener.2009.05.013.